Low energy electron-driven damage in biomolecules

L. Sanche[a]

Groupe en Sciences des Radiations, Département de médecine nucléaire et de radiobiologie Faculté de médecine,
Université de Sherbrooke, Québec, Canada J1H 5N4

Abstract. The damage induced by the impact of low energy electrons (LEE) on biomolecules is reviewed from a radiobiological perspective with emphasis on transient anion formation. The major type of experiments, which measure the yields of fragments produced as a function of incident electron energy $(0.1-30$ eV), are briefly described. Theoretical advances are also summarized. Several examples are presented from the results of recent experiments performed in the gas-phase and on biomolecular films bombarded with LEE under ultra-high vacuum conditions. These include the results obtained from DNA films and those obtained from the fragmentation of elementary components of the DNA molecule (i.e., the bases, sugar and phosphate group analogs and oligonucleotides) and of proteins (e.g. amino acids). By comparing the results from different experiments and theory, it is possible to determine fundamental mechanisms that are involved in the dissociation of the biomolecules and the production of single- and double-strand breaks in DNA. Below 15 eV, electron resonances (i.e., the formation of transient anions) play a dominant role in the fragmentation of all biomolecules investigated. These transient anions fragment molecules by decaying into dissociative electronically excited states or by dissociating into a stable anion and a neutral radical. These fragments can initiate further reactions within large biomolecules or with nearby molecules and thus cause more complex chemical damage. Dissociation of a transient anion within DNA may occur by direct electron attachment at the location of dissociation or by electron transfer from another subunit. Damage to DNA is dependent on the molecular environment, topology, type of counter ion, sequence context and chemical modifications.

PACS. 87.50.Gi Ionizing radiations (ultraviolet, X-rays, gamma-rays, ions, electrons, positrons, neutrons, and mesons, etc.) – 34.50.Gb Electronic excitation and ionization of molecules; intermediate molecular states (including lifetimes, state mixing, etc.) – 34.80.Ht Dissociation and dissociative attachment by electron impact

1 Introduction

The major impetus to investigate processes induced by low energy electrons (LEE) in biological molecules has arisen from their important role in radiobiology. The ultimate goal of the field is to accomplish a complete description of the effects of ionizing radiation in living cells and organisms by analyzing the sequence of events by which radiation modifies a biological system, and subsequently, by studying the biochemical and biological responses of this system to the transformations. This sequence of events, which eventually can lead to modifications at the molecular and cellular level, is initiated by the interaction of fast primary particles with cellular constituents. This interaction triggers a series of ultra-fast (i.e., femtosecond) events that can be divided into three major groups: primary, secondary and reactive [1]. The primary events result from the propagation of the initial high-energy particle or of

other fast charged particles produced by the primary radiation (e.g., Compton and photoelectrons). These fast particles produce excited molecules, radicals, cations, anions and secondary electrons (SE), which contain essentially all of the energy of the primaries [2]. The majority of these products have energies below 30 eV, but they are produced in large quantities $(\sim 10^5/\text{MeV})$ [3,4]. The probabilities of excitation and ionization are similar, but substantially more energy flows into ionization [2,5]. It is for this reason that SE carry most of the deposited energy.

Once created, SE also produce large quantities of radicals, cations and anions before thermalization. After having thermalized, all reactive species, whether they arise from the primary interactions or SE, can react within the irradiated system to produce new compounds and, within cells, damage biomolecules. In the vicinity of cellular DNA, these species arise from DNA itself, water and other biomolecules in close contact with that molecule such as histone proteins. In particular, the reaction with DNA of OH radicals from water radiolysis can cause

a e-mail: Leon.Sanche@USherbrooke.ca

considerable damage [6,7]. On the other hand, solvated electrons play a less significant role in such damage [8] as they primarily attack DNA bases and produce no strand breaks [6].

The primary energy deposits are now fairly well understood [5,9] and the available data serve to calculate energy absorption in biological tissue from different types of ionizing radiation [10–13]. Such data are particularly effective in calculating patient doses in radiotherapy [14] and more detailed microsimetric doses within cells [15]. There exists, however, a large gap of knowledge between our understanding of these primary events, which determine doses, and the slower chemical events responsible for the products of ionizing radiation [16]. We can determine quite precisely the energy deposited in a given volume of condensed matter but, we do not have a precise understanding and knowledge of the subsequent sequence of events, which occur within the femtosecond time scale. As a consequence, there is no well-defined relationship between adsorbed dose and the induced biological effects. To close this gap it is crucial to understand and determine the yields of processes induced by SE, particularly those driven by electrons of energy lower than c.a. $\sim$30 eV, which constitute the major portion of the SE energy distribution. It should also be noted that cellular conditions correspond to those of extremely concentrated solutions in which reactions occur within ultra short times and distances. Hence, the radiation chemistry of the cell is strongly dependent on ultra fast processes, which are in large part driven by LEE.

Our understanding of interactions between LEE ($E <$ 30 eV) and gas phase molecules arises from various electron impact experiments and theoretical advances, which have occurred over the last century [17,18]. Data on processes induced in the *condensed phase* by LEE impact have been generated later, i.e. since the eighties [19–21]. They revealed that the basic interactions found in the gas-phase were still present within molecular solids [19,20] and at surfaces [20,21], but were modified by neighboring atoms or molecules. Since the magnitude of LEE-molecule interactions is usually phase dependent [19,20], such basic information on simple condensed systems was needed to eventually understand the action of LEE in biological cells, which also constitute a condensed phase medium. The first objective of radiobiologically oriented research has been to obtain a fundamental understanding of the action of LEE within solids, composed of simple cellular molecules such as O_2 and H_2O; with the progressive development of more sophisticated technology, larger molecules of increasing complexity were investigated up to DNA [22]. Since the detrimental biological effects of ionizing radiation are usually caused by damage to the genome, most of the work related to LEE induced processes in biomolecules has been focused on DNA and its basic constituents.

The DNA molecule consists [23] of two polynucleotide antiparallel strands having the form of a right-handed helix. The strands are composed of repeated sugar-phosphate units hydrogen bonded together through the four fundamental bases, which are covalently linked to the
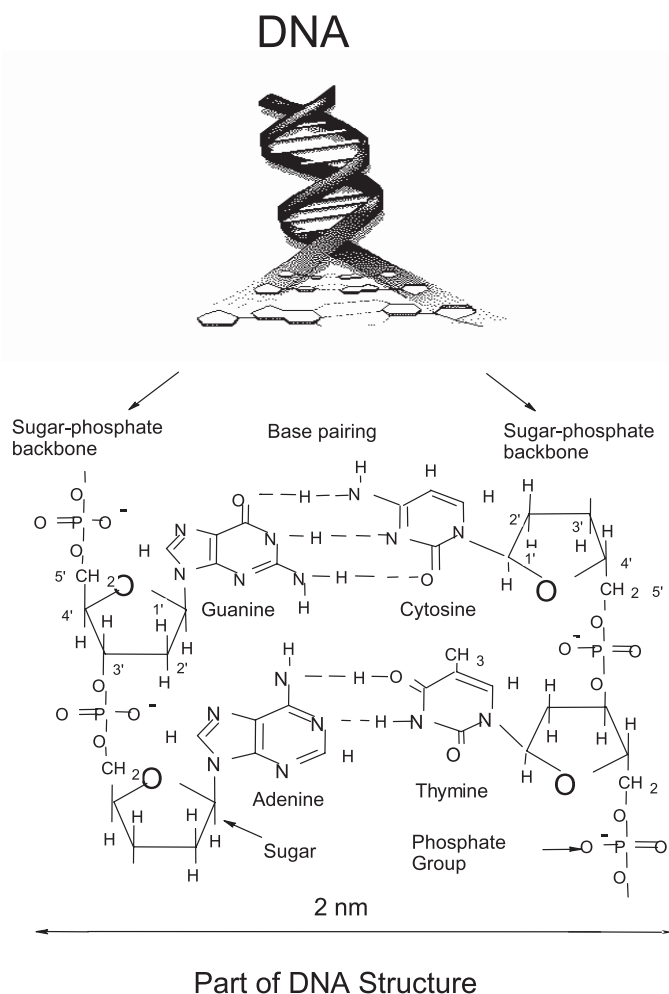

Fig. 1. Segment of DNA containing the four bases.

sugar moiety of the backbone. This is illustrated in Figure 1 for a short double-stranded segment. It consists of two sets of sugar rings with the bases guanine (G) and adenine (A), hydrogen bonded to cytosine (C) and thymine (T), respectively. Under dry conditions, DNA still contains on average 2.5 water molecules per base pair [24]. These H_2O molecules, which easily fit in the grooves of the helix, are an integral part of the DNA structure. It should also be mentioned that the negative charge on one of the oxygens of the phosphate group is counterbalanced by a cation such as Na^+. In B-type DNA, the crystallographic (averaged) structure resembles that of a twisted ladder with base pairs defining the rungs and the backbone providing the side support. The helical pitch, that is, the distance for a full turn of the helix, is 3.4 nm and there are 10 rungs per turn. The base pairs lie in a plane perpendicular to the helix axis. In A-type DNA, however, the vertical stacking is appreciably smaller. There are 11 base pairs per turn and the pitch is 2.8 nm. Moreover, in the A-type there is an important tilt of 20° of the plane of the base pairs with respect to the helix axis. In the cell, DNA is in the B form whereas in its dried state the molecule adapts the A configuration [23].

Although the first LEE impact experiment on a large biomolecule (i.e., tryptophan) was performed in 1987 by Leclerc et al. [25], a systematic investigation of cellular biomolecules was undertaken only a decade later. Results obtained since that date, both in the gas and condensed phases, are reviewed in the present article. For studies involving photoelectron emission from biomolecular anions as well as the interaction of atoms in high Rydberg states with biomolecules the reader is referred to the work of Bowen [26] and Schermann [27,28]. The theoretical efforts made to describe LEE scattering from large biomolecules are also summarized in Section 2. The most useful techniques to analyze the damage produced by LEE are described in Section 3. The experimental results obtained with large biomolecules are presented and discussed in Section 4; the conclusions are given in Section 5. A list of abbreviations is given in Table 1.

2 Theoretical results

For more than half a century, theories have been developed to explain the behaviour of cross-sections for elastic, inelastic, ionizing and dissociative processes induced by the collision of an electron with molecules of increasing complexity and size. Even though reasonably successful, these theories have until recently been limited to the treatment of relatively small molecules, usually composed of no more than a dozen atoms or so [29,30]. In fact, our theoretical description of electron-molecule scattering is still far from that needed to understand electron scattering from most biological molecules, which are usually large and complex.

A theoretical framework has recently been proposed [31,32] to describe LEE scattering from such large biomolecules, having a helical topology. The problem was decoupled into two parts: first the electron interacts with the entire molecule and then the new wave functions, defined by the atomic arrangement within the molecule, interact at a specific site of the molecule (e.g., a basic subunit). This choice was dictated by the important contribution to the scattering cross-sections arising from both resonances and electron diffraction at low energies; i.e. electron attachment requires the localization of the electron on a small subunit of the biomolecule and an electron of energy typically 5–15 eV has a wavelength that is of the order of molecular and intermolecular distances and is thus initially delocalized. In other words, the incident electron is first likely to undergo multiple intersite scattering before interacting at a specific site, where it can be captured in a resonant state. The simple model proposed consists of molecular subunits (i.e., bases, sugars, and phosphates) immersed in an optical potential U_{op}, which is constant between R-matrix shells, a working hypothesis used in the cross-section calculations for simple molecules [33] and in the theory of low-energy electron diffraction in solids [34]. The model was applied to scattering from the bases within DNA, which were represented by pseudomolecular units made of scattering centers. This application addressed the multiple scattering problem and then examined the various parameters that influence the

Table 1. List of abbreviations.

A	Adenine
Ala	Alanine
BrU	Bromouracil
BrUdR	Deoxybromouridine
C	Cytosine
Cys	Cysteine
d	Deoxyribose
D	Deuterated or deuterium
DD	Dipolar dissociation
DEA	Dissociative electron attachment
DFT	Density functional theory
DNA	Deoxyribonucleic acid
DMDS	Dimethyl disulfide
DSB	Double strand break(s)
dT	Thymidine
EEL	Electron energy loss
ESD	Electron stimulated desorption
eV	Electron volts
FWHM	Full width at half maximum
G	Guanine
GC/MS	Gas chromatography/ mass spectrometry
Gly	Glycine
HREEL	High resolution electron energy loss
keV	Kilo electron volts
LC	Liquid chromatography
LEE	Low energy electron(s) (0–30 eV)
LEEEF	Low energy electron enhancement factor
LUMO	Lowest unfilled molecular orbital
MFP	Mean free path(s)
ML	Monolayer(s)
Pro	Proline
RNA	Ribonucleic acid
SAM	Self assembled monolayer(s)
SE	Secondary electron(s)
SSB	Single strand break(s)
T	Thymine
THF	Tetrahydrofuran
Thp	Tryptophan
U	Uracil
UHV	Ultra high vacuum
UV	Ultraviolet
VAE	Vertical attachment energy(ies)
XPS	X-ray photoelectron spectroscopy

coupling of the diffracted wave to electron states localized on basic subunits. LEE scattering from A- and B-type DNA as well as that from non-periodic sequences in B-type DNA was studied. In both types of DNA, electron capture at basic sub-units was found to be considerably enhanced for some of the diffracted partial waves within DNA [31,32].

Calculations for small DNA fragments, DNA basic subunits and other simpler biomolecules were performed with more elaborate theoretical formulations. The group of Simons investigated electron attachment to several biomolecules including excised DNA fragments [35–38], using ab initio methods combined with the polarized continuum model in a self-consistent reaction field, to describe the effect of surrounding solvent or other DNA

units [35–37]. To model damage in DNA systems caused by LEE, they considered electrons that attach either to the lowest π*-orbital of cytosine and thymine or to a P=O π*-orbital of a phosphate unit. They examined a range of electron kinetic energies representative of the energy width of the lowest π*-resonance states involved and determined how the rates of cleavage of the sugar-phosphate C–O σ-bond depend on energy and on the solvation environment. In the P=O attachment study, they showed that electrons of ca. 1.0 eV could attach to form a π*-anion, which then could break either a 3' or 5' O–C σ-bond connecting the phosphate to either of two attached sugar groups. For both cytosine and thymine, the group of Simons [35–38] evaluated the adiabatic through-bond electron transfer rate with which the attached electron moves from the base, through the deoxyribose, and onto the phosphate unit and then causes cleavage of the sugar-phosphate σ-bond. Their findings show that the single strand break (SSB) rate depends significantly on the electron energy and upon the solvation environment near the DNA base. Li et al. [39] studied theoretically cleavage of this bond by direct electron attachment to a sugar-phosphate model forming a radical anion, which may live a sufficient time to subsequently induce rupture of a 3' or 5' P–O σ bond. According to the work of Berdys et al. [36, 37], 0 eV electrons may not easily attach directly (i.e., vertically) to the phosphate units as implied in the work of Li et al. [39]. Direct attachment can produce a metastable P=O π* anion, but this process would require electrons with energy >2 eV.

In their other density functional theory (DFT) calculations, Li et al. investigated bond breakage induced by LEEs in uracil (U) [40], thymine, cytosine [41], 5-halouracils [42] and adenine-halouracil base pairs [43]. From the latter, they found that dehalogenation upon electron attachment is much more efficient in isolated bromouracil (BrU); thus suggesting that DNA in which thymine has been replaced by BrU is much more vulnerable to LEE attack in the single stranded than in the double stranded configuration [43]. The potential energy surfaces they calculated via DFT for U show that the electron may attach initially to the molecule in an essentially pure π* valence state and that this state intersects with an antibonding σ* state on bond extension [40]. The bond dissociation energies were found to be lower for N–H than C–H bonds; this is explained in part by the driving force provided by the higher electron affinities of the N radical sites over the C radical sites on the pyrimidine DNA bases [40,41]. Their results imply a large hydrogen yield from these bases upon attachment of LEE [41].

Gianturco and co-workers performed quantum dynamics calculations for the scattering of LEE from U [44,45] and glycine [46]. The scattering equations were formulated within a symmetry-adapted, single-center expansion of both continuum and bound electrons, with the interaction forces obtained from a combination of ab initio calculations and nonempirical modeling of exchange plus correlation effects. Several open-channel shape resonances were obtained. For U, they predicted three resonances of

π* symmetry at energies of 2.3, 3.5 and 6.5 eV and two resonances of σ* symmetry at 0.01 and 10.7 eV [45].

Electron impact ionization cross-sections for the DNA bases and the sugar-phosphate unit of the backbone have been calculated using the Deutsch-Märk and binary-encounter-Bethe formalisms for an energy range between the ionization threshold and 1 keV by Bernhardt and Paretzke [47]. Using the latter formalism, Mozejko and Sanche [48] also calculated these cross-sections from the ionization threshold to 5 keV. Later, these authors [49] reported electron ionization cross-sections for selected analogues of components of the backbone of DNA (i.e., tetrahydrofuran (THF), 3-hydroxytetrahydrofuran, α-tetrahydrofurfuryl alcohol, phosphoric acid and the sugar-phosphate unit), using the same model. The total ionization cross-sections were found to depend on molecular symmetry, number of target electrons and molecular size. They reached maxima within the 60–90 eV range with values of the order of 2×10^{-15} cm^2, illustrating the high efficiency of 30–120 eV electrons to ionize biological targets.

3 Experimental methods

3.1 Target preparation

In gas phase experiments, the target usually consists of an effusive beam of neutral biomolecules [50]. If the compounds are easily vaporizable under vacuum, they can be leaked into an ultra high vacuum (UHV) chamber, where the beam is formed by expansion through a capillary. If the compound cannot easily be vaporized under reduced pressure, it has to be placed in an oven where it is heated to the temperature necessary to achieve the pressure needed to form an effusive molecular beam. In some cases, the biomolecules are simply introduced into a heated collision chamber [51].

In solid phase experiments, the technique of preparation is also different depending on the substance to be investigated in the form of thin films having thicknesses ranging from 0.3 to 10 nm [19,22]. Gases or liquids, having a significant vapor pressure at room temperature, can be leaked into UHV in front of a cryogenically cooled metal substrate, on which they condense. The substances that form solids at room temperature can be heated in an oven in front of the metal substrate, so as to produce a flux of molecules that condense on the metal surface. However, if the molecules cannot be heated to sublimate or evaporate without decomposing, then they must be prepared outside the UHV system in a clean environment and then introduced into the UHV chamber.

An apparatus used to measure desorbed neutral species and ion yields from electron-bombarded films of molecules, which form solids at room temperature, is shown in Figure 2 [52]. The apparatus consists of two UHV chambers. The one on the right is a load-lock chamber in which the samples are introduced. It can be pumped to a base pressure in the 10^{-9} Torr range with an oil-free turbo-molecular drag pump station, and it contains a resistively
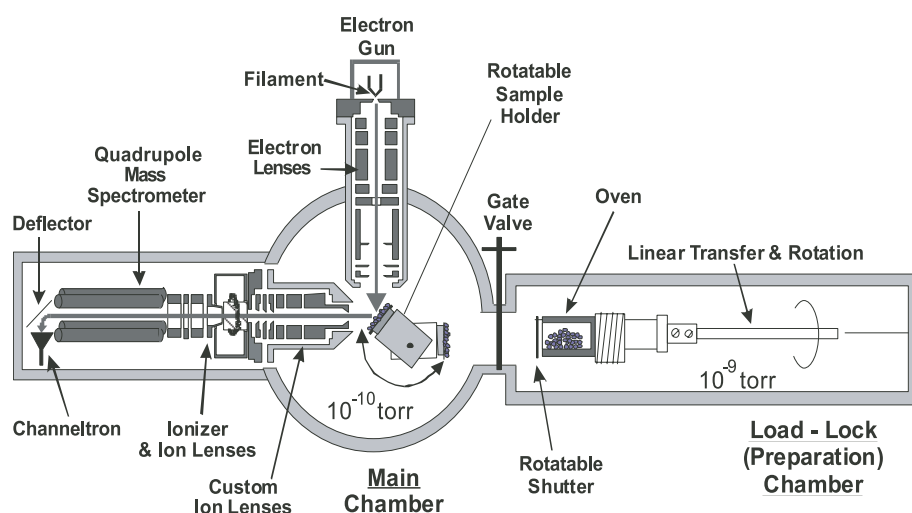
Fig. 2. Schematic overview of the type of apparatus used to investigate the desorption of ions and neutral species induced by electron impact on thin biomolecular films. The films are usually formed by the condensation of molecules leaked in vacuum or evaporated from an oven in front of a metal substrate fitted to a rotatable sample holder. From reference [52].

heated miniature oven equipped with an activated shutter. The oven can be transferred into the main chamber on the left (pressure $\sim 10^{-10}$ Torr) for vacuum deposition of a solid compound onto a polycrystalline Pt substrate held at room or cryogenic temperature. The Pt substrate is fixed to a rotatable sample holder in order to place the target in front of the electron gun and mass spectrometer. Once loaded into the oven, the sample is degassed by heating for several hours, at a temperature well below evaporation limit. The substrate is cleaned prior to each deposition by resistive heating. The integrity of the sublimated films can be verified in situ by X-ray photoelectron spectroscopy (XPS) [53] and outside vacuum by chromatography. The average film thickness is determined within 50% accuracy by measuring the mass of the condensed film with a quartz crystal microbalance [52] or by measuring the thickness-dependence of the electron current transmitted through the film during the experiment [19,52].

For compounds that might decompose by evaporation into vacuum, two different techniques have been developed to produce thin biomolecular films on metal substrates. When multilayer films are required, a solution of the compound is made and a small aliquot of the solution is lyophilized on a tantalum substrate [54]. The sample preparation and manipulation are performed within a sealed glove box under a pure dry nitrogen atmosphere. Several samples are afterwards transferred directly into an UHV system, or via a load-lock as shown in Figure 2. Samples are placed on a rotary multiple target holder, which can transport each sample in front of the LEE beam. The average film thickness is usually estimated from the amount deposited and its density [54]. It has been shown that upon adsorption onto a metal surface, certain biomolecules may chemically decompose [55,56]. Therefore, relatively thick ($\sim$5 monolayers: ML) films are usually deposited to insure that the measured signal arises from electron interaction with biomolecules lying close to the film-vacuum interface. When only a single layer of a relatively large biomolecule is needed, a clean uniform layer can be formed on a gold substrate by chemisorption, if the molecule does not fragment on the metal. This is

the technique utilized to prepare self-assembled monolayers (SAM) [57]. With this procedure, the biomolecules are chemically anchored to a gold substrate via SH groups substituted at specific positions (in DNA by substitution of the double-bonded oxygen by double-bonded sulfur atoms at certain phosphorus positions).

3.2 Measurement of ions and neutral species by mass spectrometry

Some of the damage induced by LEE impact on biomolecules can be assessed by monitoring the ions and neutral species that desorb in vacuum during bombardment. Such measurements can be performed by placing the effusive beam or sample film near a mass spectrometer, as shown in Figure 2. A LEE beam, emanating from an electron monochromator or a focusing electron gun, impinges onto the target. The full-width at half-maximum (FWHM) of the electron energy distribution varies from 0.03 to about 0.5 eV, depending on the type of electron source, for typical beam currents of 2–400 nA. In the gas phase experiments, the electron energy scale and the cross-section for ion production are usually calibrated by measuring the anion signal from a gas which exhibits a resonance at a well defined energy, and whose DEA cross-section is accurately known. Although this method provides an accurate energy calibration, it may overestimate the magnitude of the cross-sections for non volatile biomolecules, since the latter may condense on chamber walls and thus reduce their background pressure relative to the calibrating gas. Thus, many of the gas-phase cross-sections cited in this article should be considered as upper limits. Calibration on the positive ion cross-section of the same molecule could provide more reliable values [58], but direct measurement of total yields may be necessary to obtain accurate cross-sections [59]. In thin film experiments, the energy scale is calibrated such that 0 eV corresponds to the onset of electrons transmitted to the substrate [60] (i.e., 0 eV is defined as the vacuum level). This onset can be determined within an accuracy of ± 0.25 to ± 0.05 eV. Because energy shifts

in this onset are related to electron trapping, this method allows one to verify that measurements are obtained from uncharged films.

Neutral species that desorb from the films and reach the ionizer of the mass spectrometer, shown in Figure 2, can be ionized and focused onto the quadrupole rods. Charged particles are kept from reaching the ionizer by placing suitable potentials on grids or lenses located between the target and the ionizer. To increase the detection efficiency of desorbing neutral species, the latter can be ionized close to the target surface by a laser [61]. With a standard electron ionization source, the background signal can be discriminated by beam modulation lock-in techniques [62]. Such measurements do not allow determination of absolute yields. In order to determine the absolute desorption yields of neutral products from solid films, the formation of these products must be related to a pressure rise within a relatively small volume. In this case, a mass spectrometer measures the partial pressure increase in a small UHV chamber due to the desorption of a specific volatile fragment induced by LEE impact on a thin film [63].

Ions that emerge from an effusive beam or a film can be focused by ion lenses located in front of the mass spectrometer. In certain systems, the ion energies can be determined by a retarding potential or a deflector. Relative ion yields can be obtained from three different operating modes [64]: (1) the ion-yield mode, in which ions of a selected mass are detected as a function of incident electron energy, (2) the ion-energy mode, in which ions of a selected mass are measured as a function of their energies, and (3) the standard mass mode, in which the intensity of mass peaks is measured for a fixed electron energy.

3.3 Measurements by high resolution electron energy loss spectroscopy

High resolution electron energy loss (HREEL) spectroscopy, has recently been applied to probe vibrational and electronic excitations in biomolecules. With this technique [65,66], electrons leaving a monochromator are focused on a gas jet or a metal substrate on which molecules are condensed. Electrons re-emitted from the target within a narrow cone at another angle are energy analyzed by a second electron deflector (i.e. the analyzer). Depending on the apparatus, it may be possible to vary the angle of incidence or the analyzing angle or both. HREEL spectra are recorded by sweeping the energy of either the monochromator or the analyzer. The energy dependence of the magnitude of a given energy loss event (i.e. the excitation function) is obtained by sweeping the energy of both the monochromator and the analyzer with a potential difference between them corresponding to the probed energy loss. HREEL spectra are usually recorded at overall resolutions ranging from 6 to 80 meV FWHM with corresponding incident currents in the $10^{-10}-10^{-8}$ A range [65,66].

HREEL spectroscopy has also been applied to the measurement of total absolute cross-sections for fragment pro-
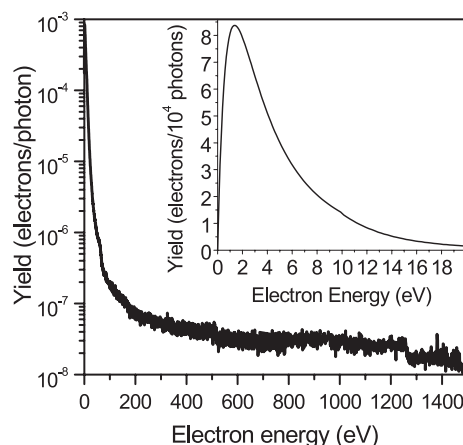

Fig. 3. Energy distribution of $Al_{k\alpha}$ X-ray induced secondary electron emission from tantalum. From reference [69].

duction by LEE impact on biomolecular films [67]. In this case, the fragments, which remain trapped within the bulk of the film, are detected and quantified in situ by recording their electronic and/or vibrational HREEL spectra [67,68]. Fragment yields are studied as a function of the electron exposure, film thickness, and incident electron energy.

3.4 Measurements of fragmentation products by X-ray photoelectron spectroscopy

As with HREEL spectroscopy, XPS can also be utilized to probe the products formed by LEE impact on thin biomolecular films. In this case, changes in the binding energy of electrons in atomic shells serve to identify fragmentation products remaining in the film. The apparatus is similar to the one presented in Figure 2, but the mass spectrometer is replaced by an electron analyzer to measure the energy of photoelectrons; a source is added to irradiate the film with X-rays. Two different types of electron sources can be used to fragment the biomolecules: an electron gun as that shown in Figure 2 or the photoelectrons emitted by the metal or semi-conductor substrate. As an example of a photoelectron electron source, Figure 3 shows the energy spectrum of $Al_{k\alpha}$ X-ray induced SE emission from tantalum; it has a peak at 1.4 eV and an average energy of 5.8 eV [69]. The spectrum was recorded with a current of 0.14 ± 0.02 nA of SE emitted from a 1.4×1.4 cm^2 tantalum substrate. The energy-integrated electron yield was 0.039 ± 0.003 electrons per photon. When the biomolecular film is sufficiently thin (<5 nm), the number of X-ray photons absorbed by the biomolecules are negligible and the induced damage may be considered to result from electrons with the energies of the distribution shown in Figure 3.

The cross-sections for electron-induced reactions are determined by assuming that the analytical XPS elemental signals from the original compound and radiation products are described by exponential functions [53]: $I_c = I_o \exp(-\sigma N t)$; $I_r = I_o [1 - \exp(-\sigma N t)]$, where I_c

a)

b)

c)

Multi-detector

Coil

Grid

Example of an
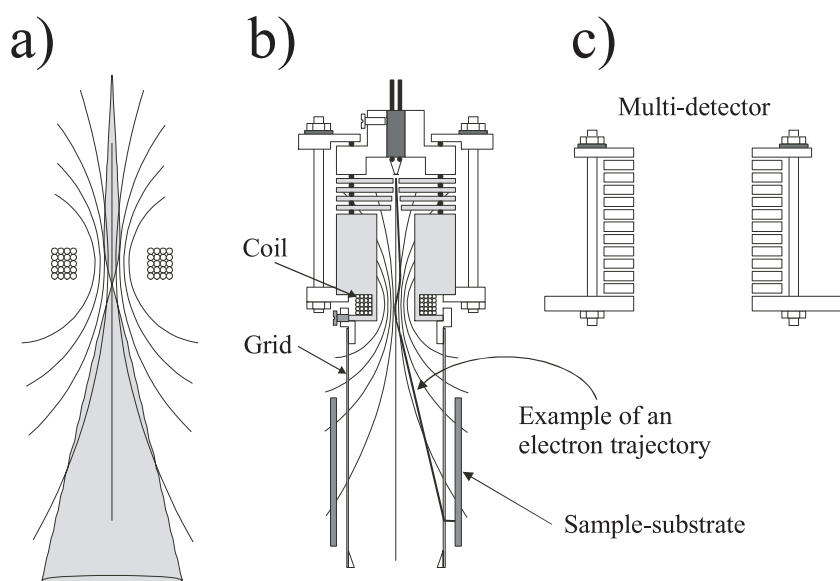electron trajectory

Sample-substrate

Fig. 4. Schematic diagram of the elements of the divergent beam low energy electron (LEE) irradiator; (a) the gradient of the non-uniform magnetic field in the electron gun, (b) cross-section view of the gun in a position to bombard the inside wall of a tantalum cylinder used as sample substrate, (c) multiple-electrode electron current detector. From reference [77].

and I_r represent the measured signals (XPS intensities) from a particular element in the original compound and the same element in the radiation products, respectively; σ is the cross-section for the corresponding process, N is the flux density of incident X-rays or electrons; t is the time of irradiation, and I_o is the maximum signal from the same element in the original compound as well as in the radiation products (i.e. measured at $t = 0$ and $t \rightarrow \infty$, respectively). Generally, measurements fit the above equations to within less than 10–15% standard deviation [53]. The validity of the above equations requires that the zone of analysis coincide with that of damage. This condition can be met for the experiments with SE from X-rays, but not with certainty for those with the electron-beam irradiation. Thus, the absolute values for the cross-sections of electron beam-induced damage may be lower than their true values. However, the relative values of the cross-sections for different compounds are much less sensitive to this effect. In principle, photons of energy lower than that of X-rays (UV and visible photons) could also be used to probe LEE induced processes within condensed biomolecules. So far, only electron trapping and transmission through short DNA oligomers have been measured with such techniques [70].

3.5 Chemical methods of analysis

In the case of complex non-volatile biomolecules, the analysis of the neutral products remaining in the film or on the metal surface after evaporation of the original compound may not be possible within UHV. The molecule may have too many degrees of freedom and energy levels to allow unambiguous identification of the in situ species by vibrational, electronic and X-ray photoemission spectroscopies. If analysis in vacuo is not possible, in principle, one could recuperate and analyze outside vacuum the products remaining on the surface by chemical methods,

such as electrophoresis [71], chromatography, gas and liquid chromatography, gas chromatography/mass spectrometry (GC/MS), liquid chromatography/MS (LC/MS) [72] or hybridization with complementary strands in the case of oligonucleotides [73]. However, for such analysis much larger quantities of fragments must be produced than in the desorption and micro-analysis experiments previously described, particularly if the yields are small (e.g. <1%).

A simple solution to these problems is to design an electron gun capable of bombarding a large area, so as to lower the density of trapped electrons, the current density, and the effects of space charge in the beam, while increasing the total current at the target and the amount of fragmented material. Another possibility is to produce only a very small amount of degraded material, with a standard electron gun [74] but find a technique to amplify considerably specific damages to the molecules. For example, in experiments with supercoiled plasmid DNA, irradiated by an electron gun focused on only a 7 mm^2 area in the energy range of 5–100 eV, the samples are retrieved from UHV and the strand breaks are analyzed by electrophoresis out of vacuum [54,75,76]. In this case, ex-vacuo detection of single and double strand breaks (SSB and DSB) in DNA is possible owing to the large amplification factor that results from the change in the topological form of the plasmid (i.e., from the supercoiled to the circular and linear configuration, respectively, when one or two strands are broken). However, such a huge amplification factor does not exist for most non-volatile molecules and biomolecules; in any case, the method is limited to a specific type of damage. Thus, the analysis of most of the non-desorbing fragments produced by LEE impact on any film consisting of large non-volatile molecules requires a more general technique.

A LEE irradiator capable of processing large quantities of non-volatile organic and biomolecules, spread out on a large surface area [77], is shown systematically in Figure 4. The biomolecules under investigation are spin coated onto

the inner surface of tantalum cylinders. Up to ten cylinders may be placed on a rotary platform housed in an UHV system, where their inner walls are bombarded by a diverging LEE beam having an absolute energy spread of 0.5 eV FWHM. Figure 4 shows the principle of operation of this irradiator. Electrons are emitted from a tantalum disk cathode and pass through the apertures at the center of four molybdenum disks electrodes (Fig. 4b). The latter serve as a defocusing electron lens to expel electrons away from the gun axis and thereby produce a divergent electron beam. Subsequently, the electrons enter an electric field free region, where a small coil produces a non-uniform magnetic field at the coil centre. The purpose of this coil is to modify the trajectories of the electrons; first by collimating them on the axis and then, in the diminishing magnetic field region, by releasing them toward a molybdenum cylindrical mesh grid. After reaching the grid, the electrons are accelerated to the desired energy by an electric field between the grid and the metal substrate. The uniformity of the electron current over the inner wall of the cylinders can be adjusted by inserting the grid into the detector, shown in Figure 4c, which is composed of 12 cylindrical electron collectors. After irradiation, the tantalum cylinders are removed from UHV and the samples are dissolved in an appropriate solvent. The resulting solution can then be analyzed by various standard chemical methods of analysis [71,72].

4 Experimental results and discussion

4.1 The DNA bases, uracil and thymidine

The first LEE scattering experiments on uracil and the DNA bases were performed by Aflatooni et al. [51] who measured electron transmission through a gas cell of these molecules. Structure in the derivative of the transmitted current indicated the presence of transient anions formed by electron attachment to π^* orbitals at specific energies for all molecules. Their work showed that the energies required to add an electron to the isolated DNA bases and the RNA base U are positive; i.e., the vertical attachment energies (VAE) are all >0 (or the vertical electron affinities are <0). The VAE of the pyrimidines T and C, differed by only 0.03 eV, whereas the VAEs of the purines G and A differed by 0.08 eV [51].

Systematic gas-phase investigations of stable anion production by LEE impact on U [58,78,79] and the DNA bases [50,80–85] provided considerable insight into the mechanisms of damage to DNA induced by SE of low energies. Electron attachment to these biomolecules leads to dissociation into various fragments without any measurable amount of stable parent anions. The fragment anions with highest abundance from U, A and the pyrimidines were $(U–H)^-$, $(A–H)^-$, $(C–H)^-$ and $(T–H)^-$, respectively as expected from theory [41]. Quantum chemical methods were used to calculate the electron affinities and binding energies of the different isomers of the $(U–H)$ and $(T–H)$ fragment [40,41,50,79]. In addition, five other fragment anions were formed by DEA to cytosine and eight
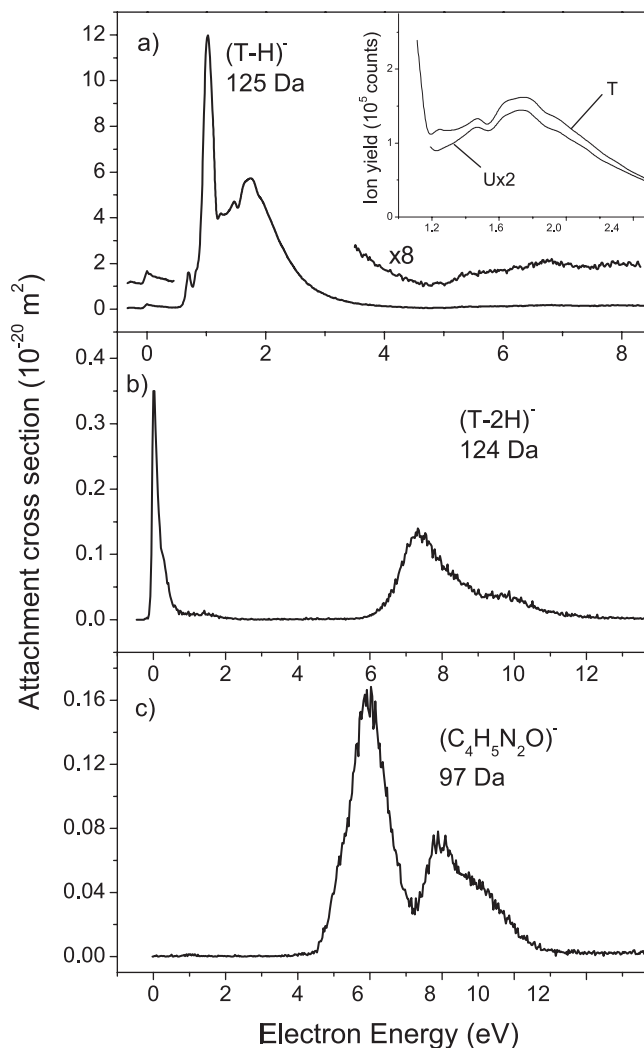

Fig. 5. Electron energy dependence of the cross-section for $(T–H)^-$, $(T–2H)^-$, and $(C_4H_5N_2O)^-$ formation by LEE impact via dissociative electron attachment (DEA) to thymine (T). The absolute scale was estimated from the known cross-section for Cl^- formation from CCl_4. The insert in panel (a) also exhibits results obtained for uracil (U). It shows the peak details in the structure of the $(T–H)^-$ and $(U–H)^-$ yield functions from about 1.1 eV to 2.4 eV. From reference [50].

additional product anions were detected in the case of thymine [50]. Yield functions were measured for all fragment anions in the electron energy range from about 0 to 14 eV. Twelve fragments were produced by DEA to uracil but with lower cross-sections than for $(U–H)^-$ [78]. Energy thresholds for dissociation into cation fragments by LEE impact on U were also determined [86]. A typical example of the numerous anions produced by LEE impact on the bases is to be found in the work of Denifl et al. [50]. Their results obtained by measuring the anions formed in a crossed electron/neutral thymine beam experiment, are shown in Figures 5–7. The anion yield functions clearly exhibits well defined peaks denoting the formation of T^- at specific energies leading to fragmentation into the anions denoted in the figures and the corresponding radicals.
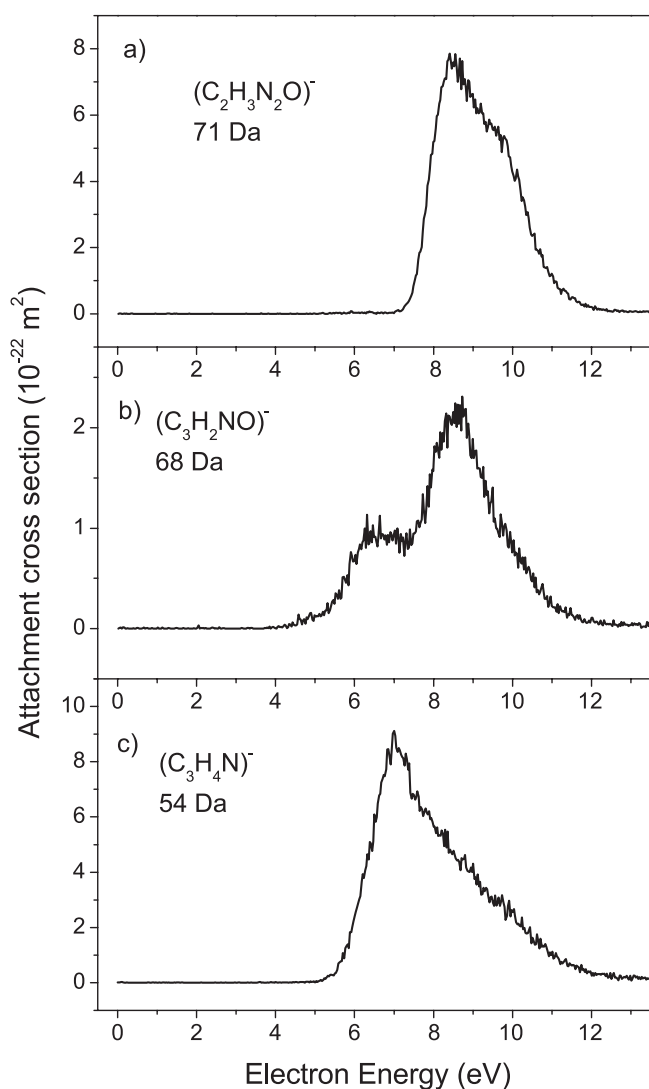
Fig. 6. The $(C_2H_3N_2O)^-$, $(C_3H_2NO)^-$, and $(C_3H_4N)^-$ DEA cross-sections obtained by 0–12 eV electron impact on gaseous thymine. The peaks denote the energy of dissociative transient anions responsible for the stable anion signal. From reference [50].
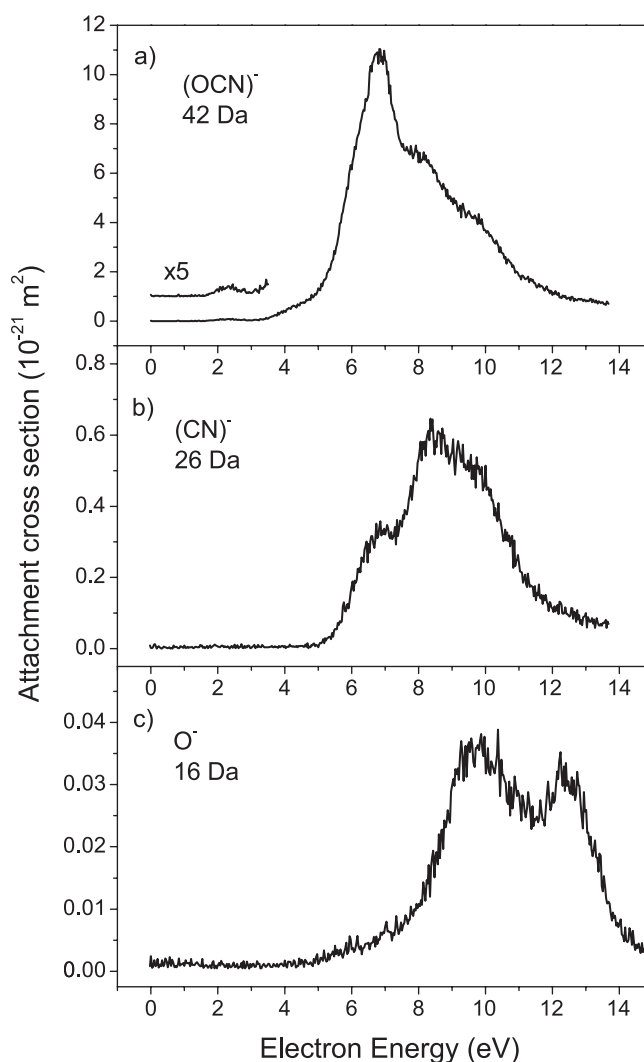
Fig. 7. Cross-sections for $(OCN)^-$, $(CN)^-$, and O^- formation by 0–14 eV electrons impinging on gaseous thymine. From reference [50].

In subsequent gaseous studies, Abdoul-Carime et al. [84] were able to show that the high hydrogen loss induced by LEE impact (e.g, Fig. 5a) on the DNA bases was site-specific. In principle, dehydrogenation of nucleobases can arise from either C–H or N–H bond cleavage. To clarify this point, these authors carried out experiments on partly deuterated (D) thymine at the carbon positions, T_D. Below 3 eV, both the energy dependence and the absolute intensity of the yield function of $(T_D-H)^-$ (129 amu) were virtually identical to those obtained from thymine $(T–H)^-$ (125 amu) [84]. By switching the mass spectrometer to mass 128 amu [corresponding to $(T_D-D)^-$], the ion signal completely disappeared. This observation provided direct evidence that DEA generates the N-dehydrogenated anion $(T_D-H)_N^-$ as confirmed by DFT calculations [41]. The structures in the $(T_D-H)_N^-$

ion yield curve suggested that different electronic states of the precursor ion are involved. Any of these states, however, decay by hydrogen cleavage from the N sites, but not from the C positions [84,85].

The four DNA bases were also investigated in the form of thin multilayer films, but fewer anions of different masses were measured than in the gas phase. The difference is principally due to the inability of the heavier anions to overcome the polarization potential that they induce in the film [87] causing them to remain trapped in the target. In fact, only the light anions H^-, O^-, OH^-, CN^-, OCN^-, and CH_2^- were found to desorb by the impact of 5–35 eV electrons on the physisorbed bases via either single or complex multi-bond dissociation [88]. The H^- yield functions exhibited resonance structures at around 9 and 20 eV, typical of DEA to the molecules. A monotonic increase in the anion yield functions was interpreted to arise from non-resonant stable-anion production via dipolar dissociation (DD). The resonance features were attributed to

electron capture by the positive electron affinity of excited states that involves the excitation of the lone-pair $n \to \pi^*$, $\pi \to \pi^*$, and/or $\sigma \to \sigma^*$ (i.e., formation of a two-electron one-hole transitory anion).

Along the same line of work, Abdoul-Carime et al. [89] investigated the fragmentation of gaseous Thymidine (dT) by LEE impact. Their results indicated that electrons with energies below 3 eV dissociate dT forming $(dT–H)^-$ and (2-deoxyribose-OH)$^-$ and $(T–H)^-$ with a break at the N1 position. These results were corroborated by measurements of the products formed in LEE bombardment of solid dT in UHV. Using the apparatus described in Section 3.5, Zheng et al. [90] were able to produce sufficient quantities of the degraded compound for analysis by high pressure LC and GC/MS. Their analysis revealed the formation of several products, thymine arising from N1-glycosidic bond cleavage of dT being the most abundant. They estimated that thymine constitutes about one third of dT decomposition at 15 eV.

Important results were also obtained at low energies from HREEL spectra of gas and condensed phase thymine. The excitation of the lowest electronic states and vibrational excitation with angular analysis in the gas phase was reported by Abouaf et al. [91]. The singlet electronic state was found to be blue-shifted by about 0.3 eV compared to the UV-visible absorption band. Evidence for a triplet state was found at 3.6 eV. The vibrational excitation modes exhibit two resonance regions, around 1–2 and 4–5 eV. The modes excited around 1–2 eV reveal an excitation of the carbonyl, CC double bond and NH stretch modes. At 5 eV, the NH stretch modes are still present but CO and CC double bond stretch modes are much less excited. Similar results were obtained for sub- and ML amounts of thymine condensed on an inert Ar surface, but only the 4-eV resonance was observed in various vibrational decay channels [92]. This broad maximum was attributed to temporary electron capture into the third anti-bonding π^* orbital of the molecule from comparison with gas-phase electron transmission data [51]. The maxima in the condensed-phase cross-sections for vibrational excitation ranged from 3×10^{-17} to 1.6×10^{-16} cm^2 depending on the excited vibrational mode.

Absolute cross-sections for electronic excitation by electron impact between 5 and 12 eV were determined for thymine deposited at submonolayer coverage on an inert Ar substrate [93]. They were derived by applying the scattering model and the experimental method originally proposed by Lévesque et al. in their electron scattering cross-section work on thin film of pyridine [94]. The lowest features at 3.7 and 4 eV in the electron energy loss (EEL) spectra of condensed T were attributed to the excitation of the triplet $1^3A'$ ($\pi \to \pi^*$) and $1^3A''$ ($n \to \pi^*$) valence states of the molecule. The higher EEL features located at 4.9, 6.3, 7.3 and 9 eV with a weak shoulder around 6 eV were ascribed mostly to the triplet valence ($\pi \to \pi^*$) excitation manifold of the molecule. The energy dependence of the cross-section for both lowest triplet valence excitations shows essentially a peak at about 5 eV reaching a value of 2.9×10^{-17} cm^2. The cross-sections

for the higher EEL features are generally characterized by a common broad maximum around 8 eV. The latter reaches a value of 1.36×10^{-16} cm^2 for the combined 6- and 6.3-eV excitation regions. The maxima in the cross-sections around 5 eV correspond to the resonances seen near 6 eV in Figures 5–7 in the anion yield functions of gaseous thymine. Interestingly, in experiments where thymine films were covered by a layer of amorphous ice, the vibrational and electronic spectra of T remained essentially unaffected, whereas formation of OH + H via the $^{3,1}B_1$ states of H$_2$O was almost completely suppressed [95].

4.2 The deoxyribose and phosphate groups of the backbone

The backbone of DNA (and also of RNA) consists of a long chain of repeated sugar-phosphate units such as those shown in Figure 1. Investigation of LEE-interaction with this unit and its two basic constituents are of special interest in relation to DNA damage. In DNA, a SSB occurs when one of the two backbones is broken. If breaks occur on two chains within a short distance ($\sim$10 base pairs or 30 Å), then the damage is referred to as a DSB. The latter damage is difficult to repair by the cell and without reparation the cell can mutate or die. To understand how such breaks can occur via LEE impact, specific sub-units of the backbone were investigated in both the gas and condensed phases. The formation of anions and cations by LEE on the gaseous deoxyribose (d) sugar ($C_5H_{10}O_4$) [96] as well as solid films of the sugar-like analogs, THF (**I**), 3-hydroxytetrahydrofuran (**II**), and α-tetrahydrofuryl alcohol (**III**) [97,98] were investigated by mass spectrometry with an apparatus of the type shown in Figure 2. In these experiments, the yield functions for H$^-$ desorbed by the impact of 1–20 eV electrons on 10-ML films were characterized by an onset at 6.0, 5.8, and 6.0 eV, and a maximum centered at 10.4, 10.2, and 10.0 eV for **I**, **II**, and **III**, respectively. Other weaker features were also observed in the H$^-$ yield functions for **II** and **III**; they appear on the low-energy side of the 10 eV peak. No other anions were observed to desorb. All features below 15 eV in H$^-$ ESD yield functions were characteristic of DEA to **I**, **II**, and **III**. A steep rise in the H$^-$ signal with an energetic threshold near 15 eV was characteristic of nonresonant DD. The formation of H$^-$ via DEA from **I**, **II**, and **III** has been discussed in detail by Antic et al. [97,98]. Owing to the strong similarity of the H$^-$ desorption profiles for **I**, **II**, and **III**, these authors concluded that the majority of the anion yield for all three systems arises from at least one transient anion associated with electron attachment to the furan ring and located near 10 eV [97]. Considering the large Rydberg character of the excited states in **I** near the energy range of the observed resonance, they further suggested that this resonant state is of the core-excited type, possibly with dissociative valence σ^* configurational mixing.

The only structural difference between compound **III** and deoxyribose is the addition of two OH radicals at the 1' and the 3' positions. However, in the case of
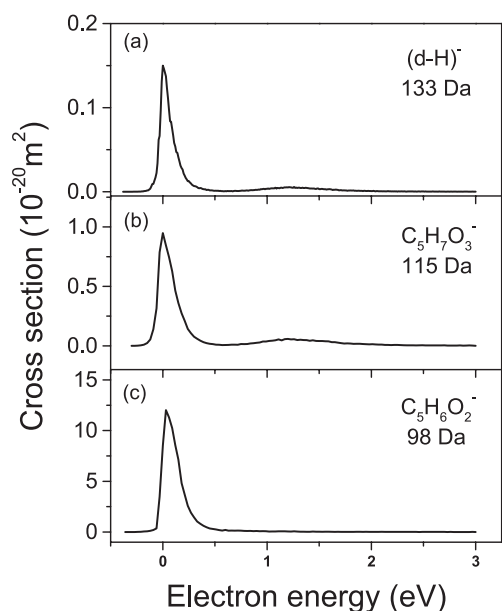
Fig. 8. Absolute cross-sections for $(d-H)^-$, $C_5H_7O_3^-$, and $C_5H_6O_2^-$ formation via DEA to deoxyribose (d) as a function of the electron energy from about 0 to 3 eV. From reference [96].

gaseous deoxyribose, anions of much larger masses were observed to be formed by LEE impact compared to similar experiments with condensed molecule **III**. As explained previously, this difference arises from the polarization field present at the surface of dielectrics. As shown in Figure 8, in their gas-phase experiments Ptasińska et al. [96] were able to observe heavy anions such as $(d-H)^-$, $C_5H_7O_3^-$ and $C_5H_6 O_2^-$. The highest measured cross-section $(1.2 \times 10^{-15}$ cm$^2)$ for the formation of stable anions from gaseous deoxyribose was observed for the fragment anion $C_5H_6O_2^-$. The mechanism leading to this anion could be interpreted as s-wave electron attachment followed by the removal of two water molecules. For $C_5H_6O_2^-$ only this resonance near 0 eV was observed. The other two fragments, $C_5H_7O_3^-$ and $(d-H)^-$ shown in Figure 8, reveal, besides a strong resonance at 0 eV, a second resonance at 1.2 and 1.5 eV, respectively, which is about 30 times lower in intensity. In contrast to the results of Section 4.1, dehydrogenation is not the predominant reaction channel for deoxyribose, but the relative amount of fragment ions compared to that of the parent cation is about an order of magnitude larger than in the case of nucleobases. This result indicates the weakness of the backbone to attack by LEE. DEA leading to the formation of $C_5H_5O_2^-$, $C_3H_5O_3^-$, $C_4H_4O_2^-$ and O^- was also observed by Ptasińska et al. within the range 0–13 eV [96]. They also measured yield functions for cation yields. The results did not reveal any particular features except for the ionization threshold of the parent at 10.51 ± 0.1 eV and thresholds for the formation of diverse positive fragments [96].

In a molecule as complex as DNA, the products of fragmentation are expected not only to involve single-step processes such as DEA, but also the reaction of the primary radicals and ions with other surrounding constituents within the molecule. The possibility of reactive scattering within the backbone of DNA has been demonstrated by Huels et al. [99] in experiments with condensed films containing O_2 and THF. Their 0–20 eV electron impact measurements show that all of the OH^- and some of the H^- desorption yields are the result of reactive scattering of the 1–5 eV O^- fragments produced initially by DEA to O_2. These O^- reactions involve hydrogen abstraction and atom exchange with THF, and result in the formation of THF-yl radicals, as well as THF oxidation products, most likely lactones and alkoxyl radicals. O^- was found to scatter over nanometer distances, comparable to DNA dimensions, and its reaction involves formation of a transient $(OC_4H_8O)^{*-}$ collision complex.

HREEL spectra of resonance-enhanced vibrational excitations of gaseous and solid THF were recorded by Lepage et al. [100]. Selective vibrational excitation enhancement for different impact energies indicates the presence of at least three temporary anion states near 4, 7.5, and 10 eV, as well as many possibly overlapping higher-lying resonances. The same technique (i.e., HREEL spectroscopy) was used by Breton et al. [67] to measure the damage induced within thin solid films of this deoxyribose analog. They reported production of aldehydes within such films condensed on a solid Kr substrate. The aldehyde fragments, which remained trapped within the bulk of the THF film, were detected in situ via their $^{3,1}(n \rightarrow \pi^*)$ and $^3(\pi \rightarrow \pi^*)$ electronic transitions and vibrational excitation modes. The production of aldehydes was studied as a function of the electron exposure, film thickness, and incident electron energy between 1 and 18.5 eV. Figure 9 shows HREEL spectra of a four-ML film of THF recorded at different times of irradiation by the electron beam ranging from zero to 0.33 min (Fig. 9b) and after 10.66–11 min of irradiation (Fig. 9a). The broad additional feature extending from 3.5 to 5.5 eV (Fig. 9a) is mostly due to formation of aldehydes. By performing such measurements at different incident electron energies as shown in Figure 9a and by quantifying the amount of aldehyde produced in the film, Breton et al. [67] obtained the energy dependence of the cross-section. Such a dependence is shown in Figure 10 for aldehyde production between 1 and 19 eV. The electron scattering cross-section is found to be 6.5×10^{-17} cm^2 between 11 and 19 eV. Its energy dependence is characterized by a small feature around 3 eV, a strong rise from 6 eV up to a maximum at 12.5 eV, followed by two structures centered around 15 and 18 eV.

Breton et al. [67] discussed aldehyde synthesis in terms of the formation of transient anion states, which may lead to the fragmentation of the molecule, to explain the structures seen in the energy dependence shown in Figure 10. The strong rise observed from about 6 eV was correlated to the electronic excitation threshold of THF which was suggested, in the solid phase, to involve electron transition to an unoccupied molecular orbital of σ^*_{CO} character. Core-excited resonances, previously identified from vibrational excitation functions in multilayer films of THF around 9 and 10 eV [100], were also suggested to contribute to the strong rise from 6 to 10 eV via the
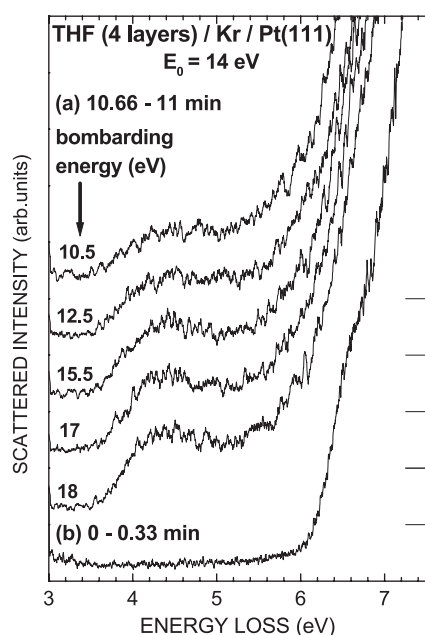
Fig. 9. Electronic-energy-loss spectra of four-layer films of tetrahydrofuran (THF) condensed on a Kr spacer film recorded during 0.33 min with 14 eV electrons: (a) following an 11 min bombardment at the energies shown and (b) on a fresh film of THF. From reference [67].
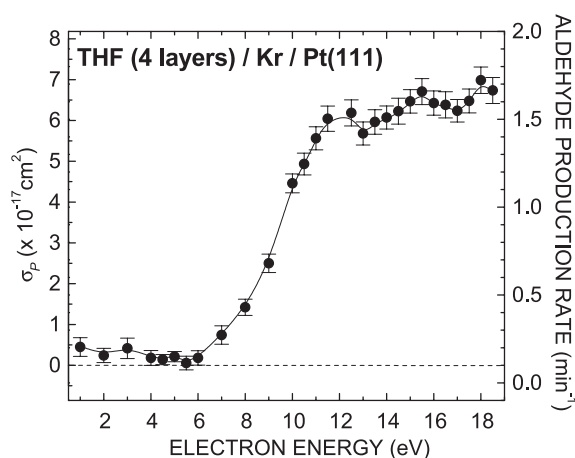

Fig. 10. Incident electron energy dependence of the cross-section σ_p (left vertical axis) and normalized rate (right vertical axis) for aldehyde production in a four-layer film of THF condensed on a Kr spacer film deposited on Pt(111). The solid line is only a guide to the eye. From reference [67].

formation of neutral dissociative states. The small feature found around 3 eV was proposed to result from a σ^* shape resonance also previously measured in the anion yields of multilayer films of THF [97], and involving the temporary trapping of an electron in either one of the two lowest unoccupied molecular orbitals (LUMO), both possessing a σ_{CO}^* character. The features seen in the energy dependence above 11 eV were explained by considering more specific core-excited resonances involving a hole in the $7b$ or $6b$, $7a$ or $5b$, and $4b$ orbitals, and two electrons in

the σ_{CO}^* orbitals. The DEA process, mentioned previously in this section [97,98], known to lead to fragmentation of THF via the formation of a core-excited resonance around 10 eV was also proposed as a possible cause of damage. Non-resonant fragmentation of THF via the formation of several cations was finally suggested to increasingly contribute to the cross-section from about 11 eV.

So far, the phosphate unit of DNA has only been investigated in the condensed phase by Pan and Sanche [101]. They reported ESD of OH^- anions from a solid film of $Na\,PO_2(OH)_2$. Their OH^- yield function exhibits a single broad peak with a maximum around 8 eV indicating the existence of an intermediate anion state leading to OH^- production, possibly via temporary electron localization in antibonding σ^* orbitals of the molecule. In trimethylphosphate [101], a surrogate for the DNA phosphate group, and in recent DFT studies of electron attachment to a sugar-phosphate-sugar unit of DNA [39], electron localization was found to occur into the lowest antibonding σ^* orbital. These results suggest the existence of a resonance at the phosphate unit resulting from a core-excited state formed by a positive ion core binding two electrons in σ^* orbitals.

4.3 Plasmid DNA

Plasmid DNA was first bombarded with electrons of energies lower than 100 eV by Folkard et al. [102] who found threshold energies for SSB and DSB at 25 and 50 eV, respectively. Later, Boudaiffa et al. bombarded with 5 eV to 1.5 keV electrons dry samples of plasmid DNA films in a supercoiled configuration [75,76,103,104]. Their samples were analyzed by electrophoresis to measure the percentage of circular and linear forms of DNA produced corresponding to SSB and DSB, respectively. By measuring the relative quantities of these forms in their 5-ML sample as a function of exposure to electrons, these authors measured the total effective cross-section ($\sim 4 \times 10^{-15}$ cm^2) and effective range (~ 13 nm) for the destruction of supercoiled DNA, at 10, 30, and 50 eV [54]. Such experiments also allowed Boudaiffa et al. to delineate the regime under which the measured yields were linear with electron exposure. It is within this regime that the incident electron energy dependence of damage to DNA was recorded more continuously between 5–100 eV [75,76,103,104]. Figure 11 shows the measured yields for the induction of SSB, DSB, and multiple DSB in plasmid DNA induced by 5–100 eV electrons. At each electron energy, the error bars in Figure 11 correspond to the standard deviation of the average reported value.

The apparent SSB yield threshold near 4–5 eV is due to the cut-off of the electron beam at low energies, whereas the DSB yield begins near 6 eV. Both yield functions possess a strongly structured signature below 15 eV and have a peak around 10 eV, a pronounced minimum near 14–15 eV, a rapid increase between 15 and 30 eV, and above 30 eV roughly constant yields up to 100 eV. In stark contrast, the multiple DSB yield has an apparent threshold near 18–20 eV and a very weak peak at 25 eV, above
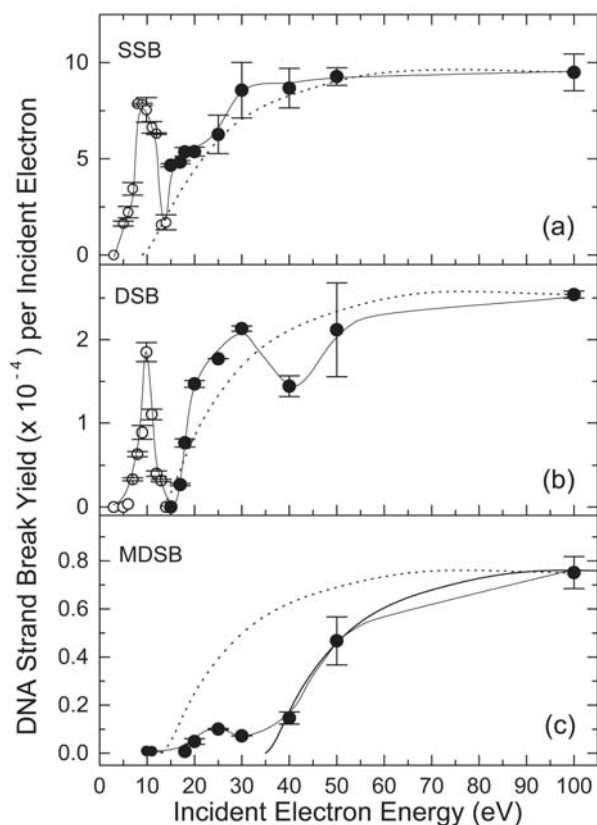
Fig. 11. Open and solid symbols are the measured quantum yields (events per incident electron) for the induction of single strand breaks (SSB) (a), double strand breaks (DSB) (b), and multiple DSB (c) in DNA films by 4–100 eV electron impact. The solid curves through the data are guides to the eye. The dotted curves symbolize general electron energy dependent signatures of cross-sections for various nonresonant damage mechanisms, such as ionization cross-sections, normalized here to the measured strand break yields at 100 eV. In (c) such a curve shifted by 30 eV is also shown (heavy solid curve). From reference [104].

Fig. 12. The H^- yield function from thin films of: (A) double stranded linear DNA, 40 base-pairs, (B) supercoiled plasmid DNA, (C) thymine, (D) ice, and (E) a deoxyribose analog. The zero-count baseline of curves A–D has been displaced for clarity. Part of a single DNA strand is shown in the left corner at the top. The dependence of the magnitude of the H^- signal on time of exposure to the electron beam is shown in the insert. From reference [105].

which it increases monotonically by about 1 order of magnitude up to 100 eV. Both peaks in the SSB and DSB yields around 10 eV incident electron energy are similar in magnitude to the respective yields above 30 eV. The relatively high yield below 15 eV may be due to electron diffraction within DNA, which amplifies the captured cross-section at specific DNA sites [32], as shown theoretically (see Sect. 2). As reported in this section, the incident-electron energy dependence of the damage to elementary constituents of DNA, probed in the form of desorbed anions and neutral species, exhibits strong variations due to electron resonances. From comparison of the maxima in the anion and neutral production yield functions of these DNA constituents to the DNA results, and from the theoretical consideration described in Section 2, it becomes quite obvious that the strong energy dependence of the DNA strand breaks below 15 eV in Figure 11 can be attributed to the initial formation of transient anions, decaying into the DEA and/or dissociative electronic exci-
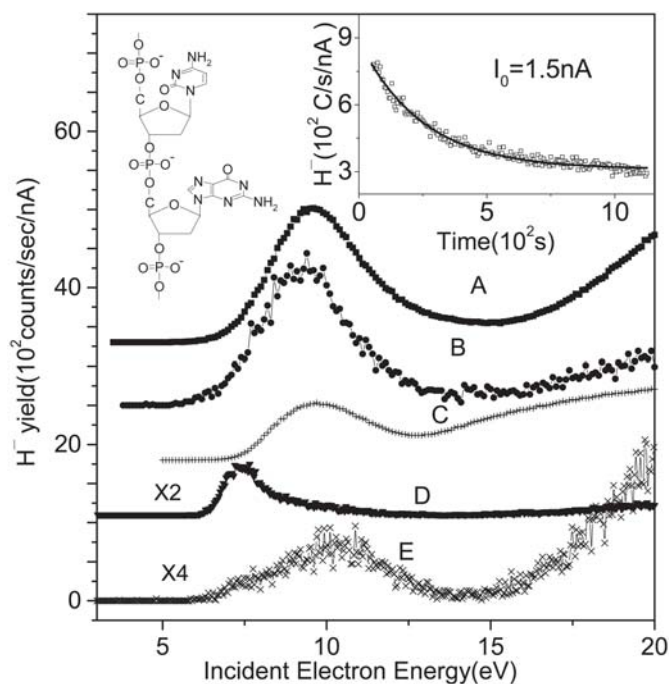
tation channels. However, because the basic DNA components (i.e., the sugar, phosphate and base units and structural H_2O) can all be fragmented via DEA between 5 and 13 eV, it is not possible a priori to unambiguously attribute SSBs and DSBs to the initial dissociation of a specific component.

A more deterministic interpretation of DNA damage below 15 eV came from the experiments of Pan et al. [105] who directly measured ESD of anions from plasmid and 40 base-pair synthetic DNA within the 3–20 eV range. Resonant structures were observed with maxima at 9.4 ± 0.3, 9.2 ± 0.3, and 9.2 ± 0.3 eV, respectively, in the yield functions of H^-, O^-, and OH^-. The yield function for H^- desorption, from synthetic and plasmid double stranded DNA is shown in Figures 12A and 12B, respectively. The yield functions for O^- and OH^- desorption exhibit a similar behavior. The prominent 9-eV feature observed in all anion yield functions is a typical signature of the DEA process. The maxima in the H^-, O^- and OH^- yield function from DNA can be correlated with the maximum spreading from 8 eV to 10 eV in the SSB yield and the one occurring at 10 eV in the DSB yield induced by LEE impact on films of supercoiled DNA (Fig. 11) [75,104]. Curves C, D and E shown in Figure 12 exhibit the H^- yield functions for desorption from films of thymine [88], amorphous ice [106], and α-tetrahydrofuryl alcohol [97]. The results obtained for the three other bases are similar to that shown for

thymine [88]. Those obtained from THF and other DNA backbone sugar-like analogs [97] are essentially the same as that shown in Figure 12, curve E. The H$^-$ peak energy from amorphous water in D is definitively too low to be associated with DEA to the structural water of DNA, unless the strong hydrogen bonding in DNA shifts considerably the H$_2$O$^-$ resonance energy. In contrast, comparison of curve C with curves A and B in Figure 12 indicates that the bases are an important source of desorbed H$^-$ with an intensity about 3 times the one arising from the sugar ring (curve E). A similar conclusion can be reached from comparison with gas-phase H$^-$/D$^-$ abstraction from the carbon position in thymine [85]. Thus, comparison of line shapes and magnitude of the yield functions in both phases suggests that LEE-induced H$^-$ desorption from DNA below 15 eV occurs mainly via DEA to the bases with a substantial contribution from the deoxyribose ring. Similar comparisons with anion yield functions from basic constituents with those of O$^-$ and OH$^-$ from DNA films [105] indicate that O$^-$ production arises from temporary electron localization on the phosphate group. The OH$^-$ desorption yield function resembles that of the O$^-$ yield, but has a considerably lower intensity. This result suggests a two step process: formation of O$^-$ via DEA to the phosphate group followed by reactive scattering of the O$^-$ ion with the nearby deoxyribose unit (i.e. reactive scattering as described in Sect. 4.2). In these ESD experiments, the counter ion on the phosphate group was Na$^+$ due to the method of preparation. Later, Pan et al. [101] studied SAM of linear single and double stranded DNA chemisorbed on a gold substrate with different orientations with respect to the substrate, and with OH groups contained within the backbone. In this case, electron impact on DNA below 19 eV produced OH$^-$ essentially via DEA to the phosphate group. Between 2 and 5 eV, this process occurred exclusively via direct DEA. Above 5 eV, direct DEA to the phosphate unit was still the dominant mechanism, but they could not rule out a possible contribution to the OH$^-$ yield, arising from reactive scattering of O$^-$. Their results showed that the phosphate-counterion part of DNA plays a significant role in LEE induced DNA damage.

It was only after the development of more sensitive techniques to detect SSB and DSB in DNA that the electron energy range below 4 eV was investigated by Martin et al. [107]. The increase in sensitivity allowed the use of only 2.0 nA electron beam currents for exposition times of samples of plasmid DNA no longer than 20 s. Under these conditions, the 0.1–5 eV range could be explored without beam defocusing and film charging. As in previous experiments, the different forms of DNA were separated by gel electrophoresis and the percentage of each form was quantified by fluorescence. Exposure response curves were obtained for several incident electron energies. As an example, the inset of Figure 13 shows the dependence of the percentage yields of circular DNA on irradiation time for 0.6 eV electrons. The amount of the linear form of plasmid DNA was below the detection limit of 0.2 ng between 0.1 and 4 eV. *Thus, induced DSBs were estimated to be less*
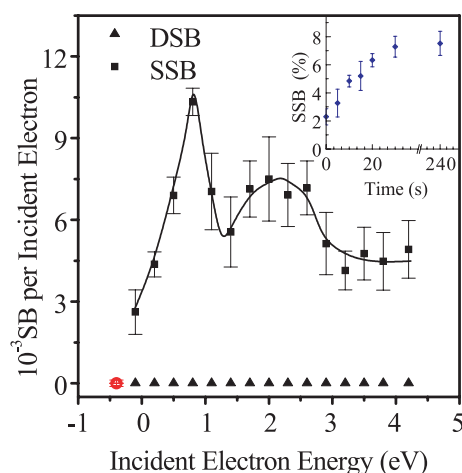

Fig. 13. Yields of SSBs and DSBs induced by 0–4.5 eV electrons on supercoiled plasmid DNA films. The inset shows the dependence of the percentage of circular DNA (i.e. SSB) on irradiation time for a beam of 0.6 eV electrons of 2 nA. From reference [107].

than one per 10^5 electrons. The yields of SSB per incident electron at each incident electron energy were determined from the amounts of circular DNA resulting from a 10 s exposure.

Figure 13 shows the dependence of the yields of SSB and DSB on incident electron energy. In total, 80 different films were bombarded and analyzed to produce these results. The error bars show the standard deviation from 3 to 8 exposure experiments, each on separately prepared samples. Two peaks, with maxima of $(1.0 \pm 0.1) \times 10^{-2}$ and $(7.5 \pm 1.5) \times 10^{-3}$ SSB per incident electron, respectively, are observed in the yield function of SSB at electron energies of 0.8 eV and 2.2 eV. The peaked structure in Figure 13 provides unequivocal evidence for the role of low lying temporary anion states in the bond breaking process. Martin et al. [107] compared their results with those described in this section from the basic DNA subunits. The curve shown in Figure 13 could be reproduced in magnitude and line shape by a model that simulates the electron capture cross-section as it might appear in DNA owing to the π^* anion states of the bases. The attachment energies were taken from the transmission measurements [51] mentioned in Section 4.1 and the peak magnitudes were scaled to reflect the inverse energy dependence of the electron capture cross-sections. Under the assumption that equal numbers of each base are resident in DNA, the contributions from each base were simply added. The lowest peak in the modeled capture cross-section, which occurs at 0.39 eV in the gas phase, was shifted by 0.41 eV to match that in the SSB yield and its magnitude normalized. Usually, in moving from the gas phase to the condensed phase, polarization effects shift the π^* resonances observed in the gas-phase to lower energies. However, in DNA the electric dipole fields created by the negatively charged phosphate groups and positive counter ions play a major role. Martin et al. [107] argued that the 0.4 eV positive shift could be explained by the phosphate charge which is closer to

the bases, thus produces a net destabilization that slightly exceeds that of the polarization induced by the transient anion.

This interpretation of electron capture by the bases below 5 eV is corroborated by direct comparison with the DEA results of Denifl et al. [50] shown in Figure 5a. In this figure, the narrow peak near 1 eV has been interpreted as due to a dipole-bound anion [108], which may not exist in DNA due to a cut-off of the long-range potential, irrespective of the value of the valence electron affinity [107]. If we assume that this is the case, the two other features in the curve in Figure 5a exhibit a good energy correspondence with the maxima in Figure 13. Thus, both comparisons offer support for the charge transfer mechanism proposed by Barrios et al. [35] discussed in Section 2 (i.e., an anionic potential surface exists that connects the initial π^* anion state of the base to a σ^* anion state of the phosphate group). The σ^* state leads to rupture of the C–O bond connecting the phosphate group to the sugar. Transport of an electron from the base to the C–O σ^* antibonding orbitals of the sugar-phosphate takes place through three saturated bonds. This is not surprising since there is ample precedence for such transfers leading to bond breaking in gas-phase DEA studies [109,110].

It is difficult to compare directly the yields obtained by LEE impact under UHV conditions, with those obtained from experiments in which DNA or other biomolecules are irradiated by high energy particles, mainly because of different experimental conditions, including the composition and conformation of the DNA. In addition, the dosimetry for LEE beam experiments is not available due to problems related to the energy imparted both to the DNA film and the metal substrate [75,76]. By using an X-ray SE emission source as described in Section 3.3, Cai et al. [69] were able to directly compare DNA damage induced by high energy photons ($Al_{k\alpha}$X-rays of 1.5 keV) and LEEs (average energy of 5.8 eV from the distribution of Fig. 3) under identical experimental conditions. In their experiments, both ML and thick (20 μm) films of dry plasmid DNA deposited on a tantalum foil were exposed to 1.5 keV X-rays for various times in an ultrahigh vacuum chamber. For ML DNA, the damage was induced mainly by the low energy SE emitted from tantalum. For the thick films, DNA damage was induced chiefly by X-ray photons. Different forms of plasmid DNA were separated and quantified by agarose gel electrophoresis. The exposure curves for the formation of SSB, DSB, and interduplex cross-links were obtained for both ML and thick films of DNA, respectively. The lower limits of G values for SSB and DSB induced by SE were derived to be 86 ± 2 and 8 ± 2 nmol J^{-1}, respectively; the average G values were about 2.9 and 3.0 times larger than those obtained with 1.5 keV photons [69].

As the energy of X-rays increases, the attenuation in ML DNA decreases, such that the contribution of SE from the metal to the yield of products becomes proportionally larger. Taking only the dose imparted by the slow SE emitted from the tantalum substrate, it is therefore instructive to define from the data of Cai et al. [69] a
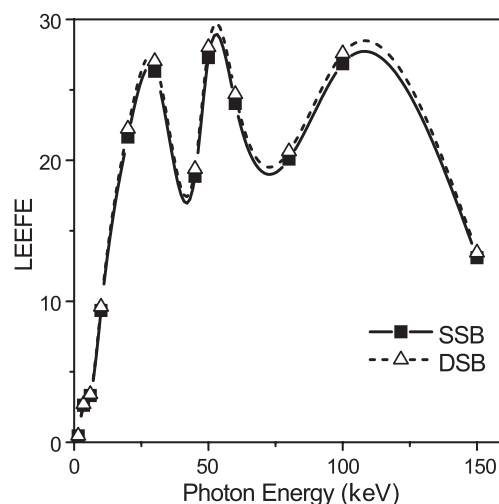

Fig. 14. Low energy electron enhancement factor (LEEEF) as a function of photon energy for SSB and DSB production in a monolayer of DNA deposited on tantalum. From reference [69].

LEE enhancement factor (LEEEF) for monolayer DNA to reflect this energy dependence. The LEEEF is defined as the ratio of yield of products in ML DNA induced by the LEE (slow SE, $E \leq 10$ eV) emitted from the metal substrate vs. the yield of products induced by the photons in a particular experiment. The LEEEF for 1.5 keV photons was derived to be at least 0.2 for both SSB and DSB, by taking average G values for SE. Extrapolation of the LEEEF at higher X-ray energies could be made by considering the X-ray absorption coefficient, the total quantum yield of LEEs on photon energy [111] and the spectrum for LEE obtained vs. photon energy [112]. The extrapolated LEEEF for X-rays from 1.5 keV to 150 keV (i.e. to energies of medical diagnostic X-rays) is shown in Figure 14. It indicates that SE electrons with the distribution and emission coefficient of Figure 3 are 20–30 times more efficient to damage DNA than the X-ray photons of 40–130 keV that create them. Dividing the values of the LEEEF of Figure 14 by the SE coefficient of Figure 3, it can be seen that when electrons with the distribution of Figure 3 strike a single DNA molecule, *they have on average a probability about 10^5 larger to damage DNA than 40–130 keV photons.* Hence, this first comparison study of DNA damage induced by X-rays and SE under identical experimental conditions shows LEE ($E < 10$ eV) to be much more efficient in causing SSB and DSB than X-rays.

4.4 Short single and double DNA strands

Further insight into the mechanisms of LEE-induced DNA damage was obtained from experiments with short single and double strands of DNA having well defined base sequences. Short DNA strands may easily be prepared as SAM chemisorbed on gold. Such samples have the advantage of being more uniform in coverage, better oriented and more pure than those made from bacterial DNA. Much of the ESD data from short single stranded
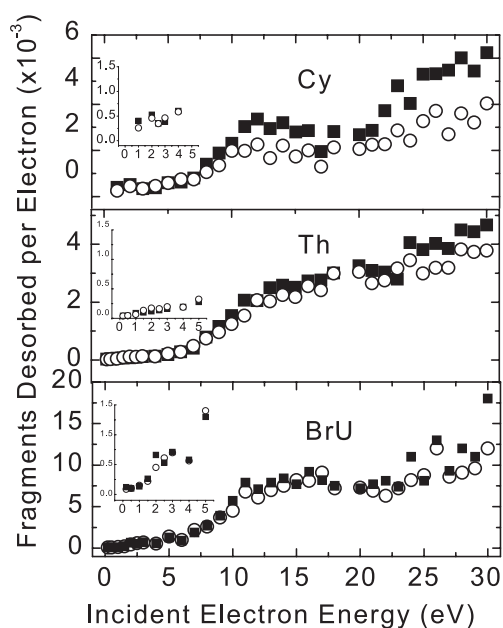
Fig. 15. Incident-electron energy dependence of neutral CN (solid square) and OCN (and/or H_2NCN) (open circle) fragment desorption yields per incident electron from C_6–$(C)_3$ (upper panel), C_6–$(T)_3$ (middle panel), and C_6–$(BrU)_3$ (bottom panel) oligonucleotides chemisorbed on a gold substrate. The spread in the data is estimated to be 20%. From reference [113].

DNA strands (i.e., oligonucleotides) have been recorded by Dugal et al. [63,113] and Abdoul-Carime et al. [114–116], who measured the yields of neutral fragments induced by 1–30 eV electrons that impinged on 6 to 12 bases SAM oligonucleotides. Their results were obtained from mass spectrometric measurements of the residual atmosphere near the target during its bombardment in UHV by a 10^{-8} A electron beam. They showed that LEE-impact dissociation of DNA bases led to the desorption of $CN^\bullet$, $OCN^\bullet$, and/or H_2NCN neutral species, as the most intense observable yields. No sugar moiety, phosphorus-containing fragments or entire bases were detected. Figure 15 presents the electron-energy dependence of neutral $CN^\bullet$ and $OCN^\bullet$ (and/or H_2NCN) fragments desorbed per incident electron from oligomers that consist of nine bases. The upper, middle and lower panels show the results from those that consist of nine cytosine bases, C_9, six cytosine bases and three thymine bases, C_6T_3, and six cytosine bases and three bromouracil bases, C_6–BrU_3, respectively. The linear increase in Figure 15 is indicative of molecular fragmentation governed mostly by non-resonant dissociation and/or dissociative ionization of the bases. Below 20 eV, a broad peak is superimposed on this linear rise. It is due to DEA and/or resonance decay into dissociative neutral states. From their data [114–116] and comparison with anion yield functions [88], Abdoul-Carime et al. suggested two possible pathways for the formation of CN and OCN by electron impact (Fig. 16): a DEA route (Eqs. (1–3)) and attack by OH radical created on adjacent bases.

From various results, such as those shown in Figure 15, it has been possible to determine effective cross-

sections or absolute desorption yields per base for base damage induced by LEE impact on homo-oligonucleotides (i.e., oligonucleotides that consist of only one type of base) [113,117]. As the strand length increased from 6 to 9 bases, a decrease in the yield per base was observed; that decrease was attributed to a greater probability of dissociation at the terminal bases [114,115]. Above nine units, no change larger than 5% of the signal was found. This percentage lies below experimental uncertainties, and the probability of fragmentation of a given base in an oligo can be considered to be constant in strands that contain ≥9 bases. Thus, these measurements provided an absolute determination of the chemical sensitivity of a base to LEE impact, in a nonamer or longer oligo. With these absolute yields, it became possible to calculate the expected yields for a specific hetero-oligonucleotide by simply adding the yields for each base contained in the strand. Such projected yields, for ≥ 9-mers oligonucleotides, necessarily *assume* that the damage is solely dependent on the chemical identity of the base, and does not depend on the environment of the base or sequence. Deviations from projected yields found experimentally would thus indicate the extent to which the environment of the bases or their sequences plays a role in DNA damage. Indeed, the experiments of Abdoul-Carime et al. showed strong deviations from the predicted yields of OCN, CN and CH_3CCO indicating that the sequence context played an important role in LEE-induced damage to the bases within oligonucleotides [114,116].

Collisions between 1–100 eV electrons and negatively charged oligonucleotides consisting of 2 to 14 bases were studied using an electrostatic storage ring with a merging electron-beam technique by Tanabe et al. [118]. The rate of neutral particles emitted in the collisions was measured as a function of 1–4 negative charges and number of bases in the oligonucleotide. The rate started to increase from definite threshold energies. These energies increased regularly with ion charges in steps of about 10 eV starting at about 10 eV for a single electron charge. They were almost independent of the length and sequence of DNA. The neutral particles came from breaks of DNA, rather than electron detachment [118]. The 10-eV step of the increasing threshold energy approximately agreed with the plasmon excitation energy [119]. From these experiments, Tanabe et al. deduced that plasmon excitation is closely related to the reaction mechanism [118].

Electron conduction [120] and temporary trapping [70] of LEE by DNA was investigated by the group of Naaman. In their experiments on LEE (<2 eV) transmission yields through SAM of short DNA oligomers [70], photoelectrons are ejected by an excimer laser operating at 193 nm (6.4 eV) from a gold substrate on which the molecules are chemisorbed [121]. The electrons transmitted through the DNA ML into vacuum are energy analyzed by time of flight. Electrons that are not transmitted are captured by DNA and transferred back to the grounded metal substrate. Because of the short lifetime of the captured electrons and the low-laser intensity and repetition rate, the ML is not charged by electrons between laser pulses. Thus,
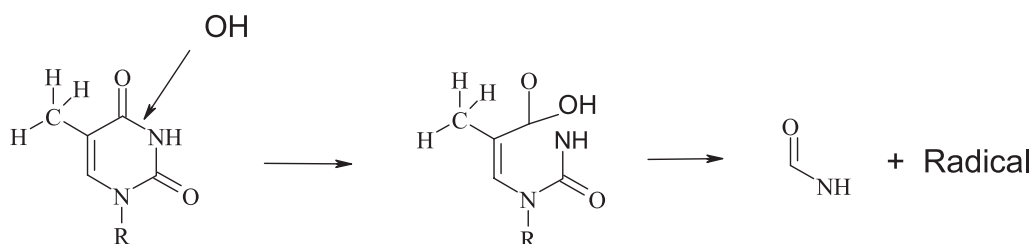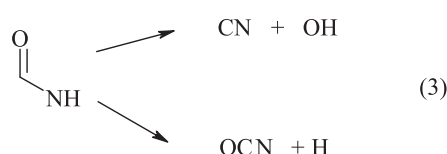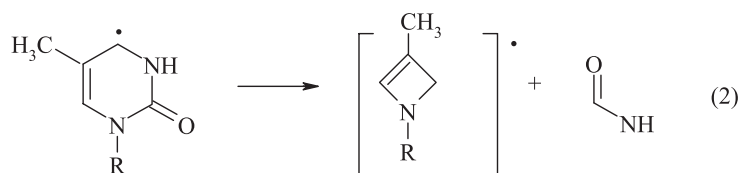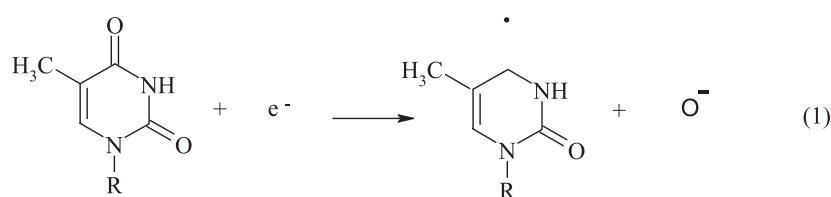
$$(1)$$

$$(2)$$

$$(3)$$

Fig. 16. Hypothetical reaction pathways for thymine ring cleavage, leading to the formation/desorption of CN and OCN neutral fragments via: (a) DEA, (b) secondary reactions induced by an OH radical created via DEA to an adjacent base. From reference [116].

the instantaneous transmitted current reflects the capturing efficiency of the layer during the duration of the laser pulse (20 μs). With such transmission experiments, Ray et al. [70] determined the dependence of the capturing probability on the base sequence and the state of the temporarily captured electrons. It was found that the capturing probability scales with the number of guanine bases in the single-stranded oligomers and depends on their clustering level.

The same experimental arrangement was used by these authors to study two-photon electron ejection from DNA SAM [70]. In this case, electrons are excited in the metal substrate with photon energy below the work function of the substrate. Some of these electrons are transferred to the LUMO of the adsorbed layer. A second photon is used to eject these electrons from the LUMO to the vacuum, where their kinetic energy is measured. The kinetic energy of ejected electrons is related to their binding energy. From such experiments, Ray et al. [70] found that, (1) once captured, the electron is not localized on one of the bases, but instead lies either on the sugar phosphate backbone or between the molecules in the ML; (2) the state of the

captured electrons is insensitive to the sequence of the oligomer and (3) double-stranded DNA does not capture electrons as efficiently as single-stranded DNA, but, once captured, the electrons are more strongly bound in the double than in the single strand configuration. Electron localization on the sugar-phosphate backbone is consistent with electron transfer from the bases leading to DNA damage [107].

4.5 The radiosensitizer bromouracil

Forty years ago, Zemenhof, De Giovanni and Greer [122] observed that bacterial cells containing DNA in which thymine has been replaced by BrU become more sensitive to ionizing radiation. This report led to an important application: the treatment of tumors by combining incorporation of halogenated pyrimidines into DNA with exposure to ionizing radiation. Since then, much work has been devoted to understand the detailed mechanisms by which such radiosensitizers operate. One of the proposed mechanisms involves the role of hydrated electrons, which are generated in aqueous irradiated biological systems.

It was suggested that these hydrated electrons first reduce the halouracil molecules to form (halouracil)$^-$, followed by dissociation of this anionic species into the corresponding stable halogen anion and the reactive uracil-5-yl radical [123,124]. These reactive radicals then enhance DNA damage and strand breaks [125,126]. Thus, the substitution of the CH$_3$ group in thymine by a halogen atom may substantially enhance radiation damage to DNA via its reaction with thermalized electrons.

Following early investigations with solvated electrons, a relatively large number of experiments have been performed both in the gas [81,91,108,127–130] and condensed phases [53,131,132] to study the interaction of LEE with halogenated pyrimidines. Similar experiments were also performed with SAM of BrU-substituted oligonucleotides [113,114,117]. Measurements have included, not only mass spectrometric detection of the yields of ion and neutral species induced by LEE-impact, but also recordings of electronic and vibrational HREEL spectra from gaseous BrU [91]. All experiments with BrU clearly indicated that the radiosensitivity of BrU is much more complex than previously anticipated. Resonant electron mechanisms lead to complex molecular decompositions over the entire electron energy range between 0 and 7 eV, and induce formation of different anion and radical fragments (compared to T) via different dissociation pathways. If formed within DNA, some of these fragments may react and thus lead to lethal clustered damage in addition to that already occurring in unsensitized DNA.

Enhancement of LEE-induced damage by substitution of CH$_3$ by Br in thymine can readily be seen in the lower panel of Figure 15, which exhibits the CN and OCN desorption yields from a BrU-substituted oligonucleotide SAM. The magnitude of the signal within the 5–15 eV range is about four times that measured with the thymine oligonucleotide. Furthermore, an extra peak is observed at 3 eV for the BrU-substituted oligonucleotides in the inset at the bottom of Figure 15. Because this peak lies at an energy too low to involve any electronically excited states, it was assigned to the formation of a shape resonance that consists of the BrU molecule in the ground state with an electron that occupies a usually unfilled orbital. The data of Figure 15 corroborated those obtained in XPS investigations [53], where LEE impact was found to dissociate bromouracil below 5 eV via resonant-electron capture by BrU followed by dissociation into a uracil-yl radical and Br$^-$.

Perhaps the most striking evidence of the huge enhancement of LEE damage obtained from Br substitution lies in the original results of Klyachko et al. [53] shown in Figure 17. The bottom curve was recorded from an unirradiated ∼100 Å film of BrU, the upper curve by exposure to 2×10^{16} e^-/cm^2 of 3 eV and the others by exposure to 6×10^{16} photons/cm^2. The peak at 72.0 eV binding energy corresponds to the photoelectron distribution emitted from the Br(3d) level. The curve labelled Dry/X-ray was obtained from the same film bombarded essentially by the SE emitted from the MoS$_2$ substrate. It exhibits an additional peak at 69.4 eV corresponding to
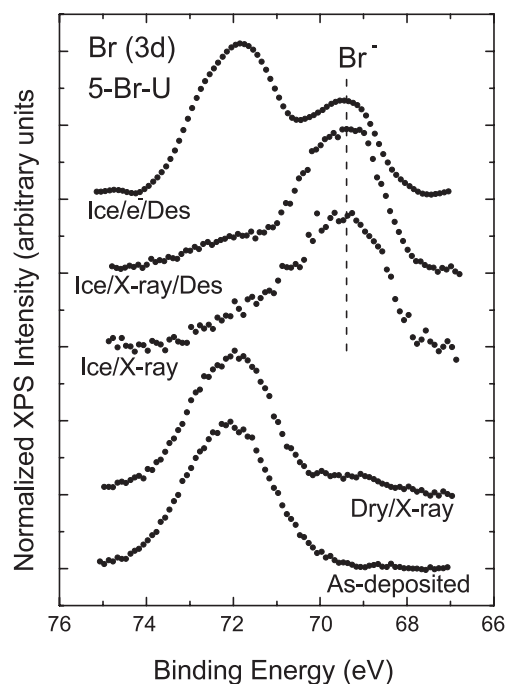

Fig. 17. The XPS spectra of Br (3d) and Br$^-$(3d) levels in 5-BrU from (bottom to top) a: freshly deposited dry film, dry film irradiated with X-rays, wet film irradiated with X-rays, wet film irradiated with X-rays and measured after water desorption, and wet film irradiated with electrons and measured after water desorption. From reference [53].

the Br$^-$(3d) level. The two other curves labelled Ice/X-ray and Ice/X-ray/Des were obtained from ∼100 Å films made of intercalated alternative layers of water ice and BrU. In this case, the X-ray Br(3d) signal almost completely disappears and is replaced by the signal from the Br$^-$(3d) level. To produce the Ice/X-ray/Des and Ice/e$^-$/Des curves, the H$_2$O molecules were evaporated from the sample before analysis. Using the method described in Section 3.4, Klyachko et al. [53] estimated from these results the effective cross-sections for Br$^-$ production. For the dry samples they obtained a value of 0.9×10^{-18} cm^2, which increased to 2×10^{-16} cm^2 for LEE bombardment of wet samples. Furthermore, a lower limit of 10^{-15} cm^2 can be estimated from their data for Br$^-$ formation via SE electron interactions, assuming a distribution of SE similar to that shown in Figure 3. Thus, the results of Klyachko et al. clearly show that DEA to BrU and other halogenated pyrimidines bases [53] very effectively produce a corresponding highly reactive radical (e.g. uracil-yl in the case of BrU) when the molecules are embedded in a water ice environment.

Since the experiments of Klyachko et al., the gas-phase mass spectroscopy investigations of the halogenated pyrimidine bases [81,91,127–130] have definitively identified transient BrU$^-$ below 2 eV, which dissociates into the fragment ions Br$^-$ and uracil-yl with cross-sections up to the 10^{-14} cm^2. More recently, radiosensitization has been demonstrated from anion mass spectrometry measurements of LEE bombarded gaseous 5-bromouridine (BrUdR) [133], which is composed of bromouracil-yl

linked to the DNA sugar moiety at the C1 position. Besides formation of the expected Br^-, BrUdR dissociated into the sugar, (2-deoxyribose-yl)· and the 5-bromouracil-yl anion. The cross-sections for the formation of the latter and Br^- were measured to be 9×10^{-16} cm^2 and 2×10^{-14} cm^2 [133]. Negative fragment ions were also observed at higher energy but with an appreciably lower intensity. They arose from more complex dissociation pathways, involving molecular re-arrangement during the lifetime of the transient ion $(BrUdR)^-$.

In conclusion, the sensitization properties of halouracils are related not only to hydrated electrons, but also to free low energy SE via DEA. However, according to theory [43], the high propensity of LEE to fragment BrU and BrUdR at very low energy (<1 eV) may only exist in single stranded DNA. This theoretical prediction was recently confirmed for the case of solvated electrons by Cecchini et al. [134]. Single and double stranded oligonucleotides as well as DNA containing mismatch bubble regions were irradiated with γ-rays in a solution where the different radicals produced could be controlled by scavengers. Such a control enabled these researchers to investigate the action of solvated electrons and determine the effects of BrUdR substitution for thymidine in these DNA targets. *BrUdR did not sensitize complementary double stranded DNA, but it greatly sensitized single stranded DNA.* However, when the BrUdR was present in a single-stranded bubble of a double-stranded oligonucleotide, the non-base paired nucleotides adjacent to the BrUdR as well as several unpaired sites on the opposite unsubstituted strand were strongly sensitized. Since LEE (<1 eV) and solvated electrons fragment BrUdR by the same fundamental DEA mechanism [123,133], these results suggest that the strong radiosensitizing action at electron energies below 1 eV is likely limited to single strand regions, as those found in transcription bubbles, replication forks, DNA bulges and the loop region of telomeres. These findings may have profound implications for the clinical use of BrUdR as a radiosensitizer as well as for the development of targeted radiosensitizers [134,135]. The damage resulting from the presence of BrUdR in the parental strand at replication forks during irradiation should be distributed randomly in the genome in a population of asynchronously replicating cells. However, in the case of transcription and telomeres, the damage should be targeted to actively transcribed genes and to the ends of chromosomes, respectively, independent of the phase of the cell cycle [134].

4.6 Protein subunits: amino acids and peptide and disulfide bridges

Within cells, histones and the other chromosomal proteins are in close contact with DNA. It is therefore possible that the radicals produced from SE, may not only denature proteins, but may also induce reactions with nearby nucleic acids. Thus, from a radiobiological point of view, there is considerable interest in studying the fragmentation of chromosomal proteins induced by LEE. Unfortunately, the complexity of protein structure does not presently allow a direct detailed analysis of the mechanisms that underlie the fragmentation processes. Research has therefore been focused on the investigation of the action of LEE on protein sub-units, more particularly on amino acids and the peptide and disulfide bonds.

The first LEE impact experiment on an amino acid was performed by Leclerc et al. [25], who measured low energy electron transmission spectra from thin solid films of Triptophan (Trp) of different thickness (9–16 Å). Their data were analyzed with the aid of a simulation model of electron transport in condensed media, which allowed an estimation of LEE scattering mean free paths (MFP) in a biological solid. They obtained a total MFP varying from 4.3 to 8.5 Å within the 0–16 eV range and a MFP for electronic excitation varying from 280 Å to 90 Å above threshold. From these values they derived the total and electronic excitation electron scattering cross-sections per molecule in solid Trp (σ_{tot} and σ_{elec}), to be 3.1×10^{-15} cm^2 $< \sigma_{tot} <$ 6.1×10^{-15} cm^2, and 0.9×10^{-16} cm$^2 < \sigma_{elec} < 3.1 \times 10^{-16}$ cm^2, respectively.

Following this work, electron transmission spectra were recorded in the gas phase by Aflatooni et al. [136]. VAE for the formation of low-lying temporary anion states of glycine (Gly), alanine (Ala), phenylalanine, Trp, proline (Pro) and cysteine (Cys) were found to be 1.93, 1.80, 0.87, 0.68, 1.91 and 0.98, respectively. The temporary anion states near 1.9 eV were formed via electron attachment into the empty π^* orbital of the –COOH group. Assignments were supported by the results of ab initio self-consistent field calculations of the lower virtual orbital energies of the amino acids [136].

The peptide and disulfide bonds of proteins can be modeled by acetamide (CH_3CONH_2) and dimethyl disulfide [DMDS:$(CH_3S)_2$], respectively. Abdoul-Carime et al. [137,138] reported measurements of low-energy ESD of anion fragments from acetamide and DMDS films. Non dissociative electron capture by disulfide bonds was also observed [139]. Electron irradiation of physisorbed CH_3CONH_2 produces the negative fragments H^-, CH_3^-, and O^-, whereas the H^-, CH_2^-, CH_3^-, S^-, SH^-, and SCH_3^- anions desorb from DMDS films. Below 12 eV, the dependence of the anion yields on the incident electron energy exhibits structures indicative of fragmentation via DEA. Within the range 1–18 eV, 1.7 and 1.4×10^{-7} H^- ion/incident electron and (7.8×10^{-11} and 4.3×10^{-8}) of the other ion/incident electron desorb from acetamide and DMDS films, respectively. These results suggest that, within proteins, the disulfide bond is much more sensitive to LEE attack than the peptide bond.

Further measurements of the ESD of anions were reported for thin condensed films of the amino acids Trp, histidine (His), Pro [140], Gly, Ala and Cys [141] multilayer films physisorbed on a Pt substrate. H^-, O^-, OH^- and CN^- desorb from Trp, His and Pro, whereas CH_2^- is observed only from Pro fragmentation. (H^-, CH^-, CH_2^-, CH_3^-, O^-, OH^- and CN^-), (H^-, CH_2^-, CH_3^-, O^- and OH^-), (H^-, O^-, OH^- and CN^-, S^- and SH^-) anions desorb from Gly, Ala and Cys, respectively. The energy averaged yields measured at the detector of the mass
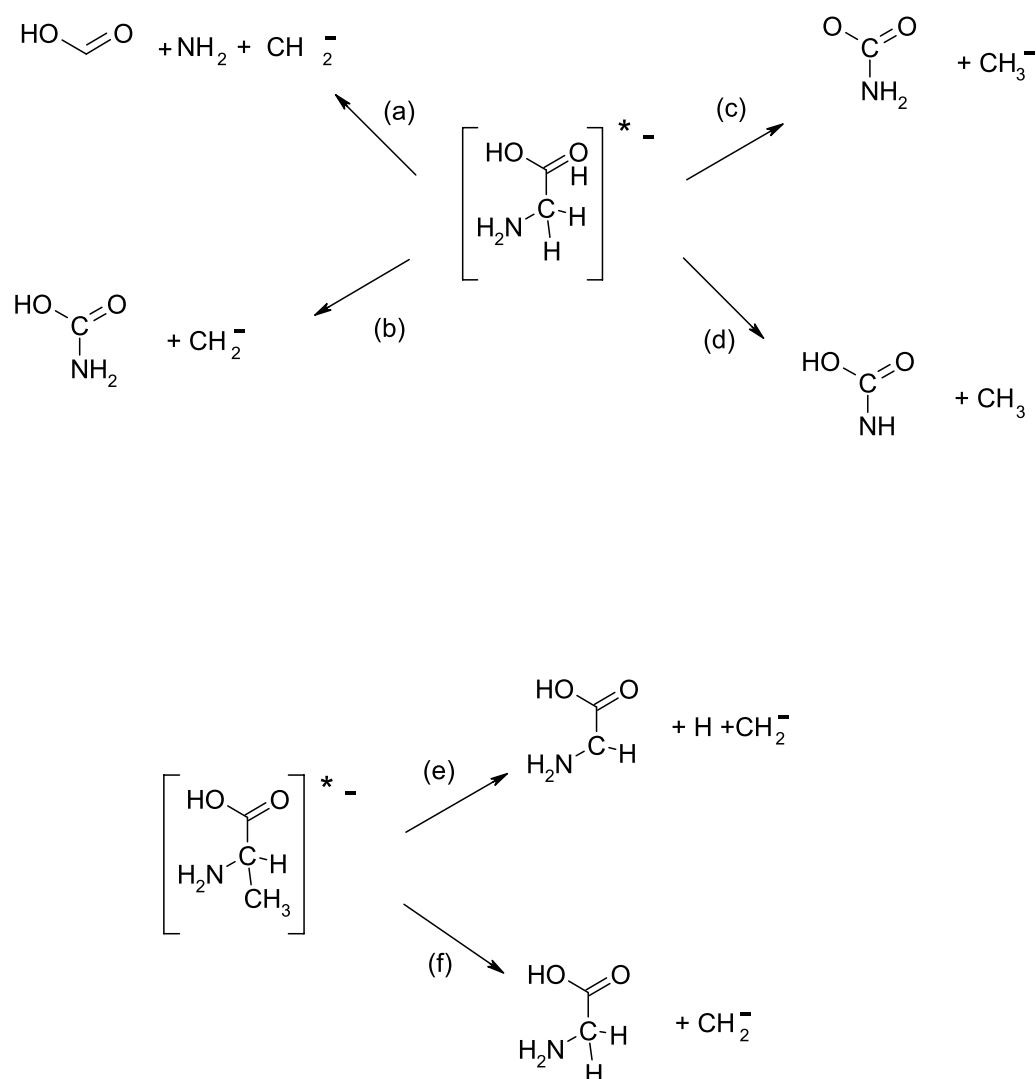
Fig. 18. Possible dissociation pathways for (a, b) CH_2^- and (c, d) CH_3^- production after low-energy electron attachment to glycine. Reactions (e) and (f) represent possible pathways for fragmentation into CH_2^- and radicals from alanine. Interestingly, via reaction (f) alanine is transformed into glycine. From reference [141].

spectrometer were $(4.9, 0.3 \text{ and } 54.0) \times 10^{-8}$ H$^-$/incident electron from Trp, His and Pro dissociation. Fragmentation of these amino acids was found to be as intense as that of the nucleic acid bases. All anion yield functions exhibit structures at energies below 15 eV, indicating that molecular dissociation operates via DEA. Above 15 eV, anion desorption is dominated principally by non-resonant DD. However, with the exception of Trp and His, an additional structure observed at 20 eV in the yield function of H$^-$, denotes the presence of another resonant process: DEA and/or decay of a transient molecular anion into the DD continuum or both [140,141]. The presence of the sulfur group in Cys was found to enhance dissociation by two orders of magnitude, relative to Gly and Ala. For example, excluding H$^-$, the average desorbed anion yields from the fragmentation of Gly, Ala and Cys were estimated to be $(5.5, 9.0, 363) \times 10^{-10}$ ion/incident electrons. Considering that cysteine also produces the highest H$^-$ yield, it is clear that according to these yields, Cys is the most sensitive of the investigated amino acids to LEE attack.

The decay of anions formed by the temporary binding of an electron to biomolecules such as amino acids and the DNA bases are usually more complex owing to the large number of possible channels for DEA and autoionization. As shown on top of Figure 18 for the case of Gly, fragmentation of (Gly)$^-$ operates via competitive dissociative pathways [141]. The transient (Gly)$^-$ anion may decay along a specific coordinate of a repulsive potential energy surface, up to crossing points where the different dissociative channels (a) to (d), may become accessible. In the case of a concerted reaction, displacement of a hydrogen atom for instance, would lead to the formation of a methyl anion as shown by reaction (c) and (d). Reactions (e) and (f) represent possible pathways of CH_2^- fragmentation from alanine. Interestingly, via reaction (f), alanine is transformed into glycine.

Gas phase investigations of LEE induced damage to protein subunits have been reported for the amino acids Ala [142], Trp [143], Gly [144,145], Pro [146] and Cys [147]. As in the case of DNA constituents, heavier stable anion fragments could be observed by mass spectrometry in this phase. For all cases, the anion yield functions exhibited purely resonant behavior indicating that the formation of transient anions was the sole mechanism
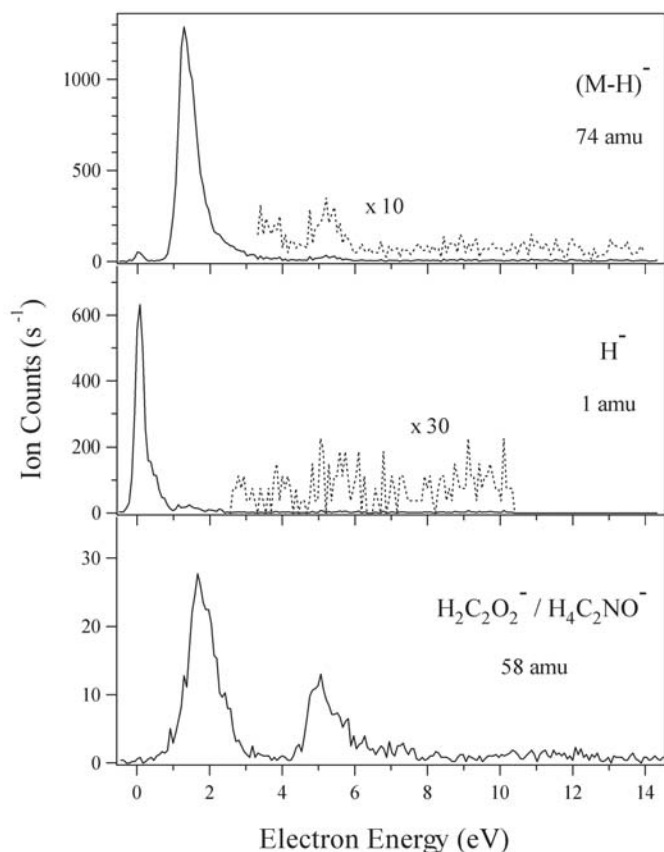
Fig. 19. Yields for three fragment anions desorbed from glycine as a function of electron energy. The closed shell anion $(M–H)^-$ formed at low energy (<3 eV) has the nomenclature $(H_2NCH_2COO)^-$. From reference [144].

responsible for the anion signal observed below 15 eV. In the case of gaseous Ala, Pro and Gly, the most intense product was the dehydrogenated anion. It is the dehydrogenated Gly anion $(H_2NCH_2COO)^-$, which appears as a low-energy resonance peak located at 1.4 eV on top of Figure 19 [144]. The cross-section for its production lies in the range 10^{-16} cm^2. For Ala and Gly, precursor Ala$^-$ and Gly$^-$ to dehydrogenation can be characterized by electron attachment into the empty π^* orbital of the –COOH group as assigned from electron transmission experiments and calculations of Aflatooni et al. [136]. At the bottom of Figure 19, the Gly$^-$ state is also seen to decompose into a neutral radical and a negative ion fragment with 58 amu. The peak near 1.8 eV was attributed to anions of the stoichiometric composition $H_2C_2O_2^-$ or $H_4C_2NO^-$. Since the energetically most favorable channel yielding H$^-$ has a threshold of 2.8 eV, the H$^-$ signal in Figure 19 could not be attributed to a primary DEA reaction near zero eV. The possibility of secondary reactions was invoked but the origin of the H$^-$ signal remains unclear [144]. A further prominent DEA peak, observed at 6 eV in other anion yield functions of Gly, was found to lead to the desorption of at least six different negative ion fragments with mass numbers: 16 amu (O^-/NH_2^-), 17 amu (OH$^-$), 26 amu (CN$^-$), 28 amu (H_2CN^-), 45 amu

(HCO_2^-), 56 amu $(H_2C_2NO^-)$. In gaseous cysteine [147], DEA below 10 eV leads to the formation of (Cys-H)$^-$, O$^-$ and/or NH$_2^-$, S$^-$ and SH$^-$ as well as their respective neutral counter-parts. In the amino acids, molecular fragmentation arise from simple bond cleavage (e.g. Cys-H)$^-$, SH$^-$) or more complex reactions involving substantial reorganization of the nuclei within the lifetime of the transitory anion [143,147].

5 Conclusions

The results of LEE impact experiments on protein subunits, single and double stranded DNA and its basic constituents as well as halogen substituted thymine and thymidine were reviewed in this article. With the exception of vitamin C [148], no other type of biomolecules appear to have been studied by LEE impact to date. Details of LEE interactions with these biomolecules obtained from different experiments, performed in both the condensed and gas phases, and theoretical calculations provide a number of common observations. We can therefore arrive with considerable certainty at the following conclusions on LEE-induced damage to the biomolecules that have been investigated so far: (1) below the threshold for dipolar dissociation ($\sim$15 eV) bond rupture occurs essentially via the formation of transient anions decaying into dissociative electronically excited states or into the DEA channel; (2) above the DD threshold rupture occurs via direct scattering but transient anions can also play a significant role up to energies of about 40 eV; (3) the induced damage depends on the environment of the molecule which inevitably modifies the lifetime of transient anions; (4) the magnitude of bond cleavage can be considerably increased by substitution with an halogen atom and (5) reactive scattering of anions formed by DEA gives rise to secondary products. Reactive scattering occurs within DNA, where it leads to OH$^-$ formation from the backbone. By this mechanism, DEA causing a break on one strand can produce a radical or anion that will reactively scatter on the other strand, thus causing a double strand break [103]. In DNA, not only the environment, but also the topology affects the damage. More generally, the results obtained may, in certain experiments, depend on the purity of the DNA, its different forms, packing of the layers and the method of preparation. For example, depending from which solution DNA is prepared the phosphate-counter ion can be different. As a consequence, different product yield functions could be observed in ESD experiments.

Since SE of low energy possess a large portion of the energy deposited by high energy radiation, any modification of their energy deposits at crucial cellular sites is expected to have a strong radioprotective or radiosensitizing action. Thus, parameters that affect LEE-induced DNA damage are of relevance to radiosensitivity and *the mechanism involved must be well understood to achieve biological control of ionizing radiation*. This has been well demonstrated in the case of bromouridine: not only was it important to unravel the basic mechanisms responsible for radiosensitization, but more biochemical experiments were

necessary to determine the role of strandiness in cellular DNA [134]. This example points out the need for multi-disciplinary studies in this field and its potential for applications to therapy combining chemotherapeutic agents, radiosensitizers and radiation.

References

1. L. Sanche, Radiat. Phys. Chem. **34**, 15 (1989)
2. M. Inokuti, *Atomic and Molecular Data Needed for Radiotherapy and Radiation Research* (TECDOC-799, IAEA Press, Vienna, 1995)
3. U. Uehara, H. Nikjoo, D.T. Goodhead, Radiat. Res. **152**, 202 (1999)
4. J.A. LaVerne, S.M. Pimblott, J. Phys. Chem. **99**, 10540 (1995); J.A. LaVerne, S.M. Pimblott, Radiat. Res. **141**, 208 (1995)
5. M. Inokuti, Rev. Mod. Phys. **43**, 297 (1971)
6. C. von Sonntag, *The chemical basis for radiation biology* (Taylor and Francis, London, 1987)
7. C. Chatgilialoglu, P. O'Neill, Exp. Gerontol. **36**, 1459 (2001)
8. S. Gohlke, E. Illenberger, Europhys. News **33**, 1 (2002)
9. N.F. Mott, H.S.W. Massey, *Theory of Atomic Collisions* (Clarendon, Oxford, 1965)
10. M. Bardies, P. Pihet, Cur. Pharm. Design **6**, 1469 (2000)
11. D. Goodhead, H. Nikjoo, Int. J. Radiat. Biol. **55**, 513 (1989)
12. A. Ahnesjo, M.M. Aspradakis, Phys. Med. Biol. **44**, R99 (1999)
13. W.R. Holley, A. Chatterjee, J.L. Magee, Radiat. Res. **121**, 161 (1990)
14. J.L. Horton, *Handbook of Radiation Therapeutical Physics* (Prentice-Hall Inc., New Jersey, 1987)
15. H.H. Rossi, M. Zaider, *Microsimetry and its Applications*, (Springer, New York, 1994), Chap. VII
16. Research Needs and Opportunities in Radiation Chemistry Workshop, DOE Final Report SC-0003, US Department of Energy (1998)
17. L.G. Christophorou, *Electron-molecule interactions and their applications* (Academic Press, Orlando, 1983), Vol. 1 and 2
18. H. Hotop, M-W. Ruf, M. Allan, I.I. Fabrikant, Adv. At. Mol., Opt. Phys. **49**, 85 (2003)
19. For a review see L. Sanche, in *Excess electrons in dielectric media*, edited by J.-P. Jay-Gerin, C. Ferradini (CRC Press, Boca Raton, 1991)
20. For a review see A.D. Bass, L. Sanche, in *Charged particle and photon interactions with matter: Chemical, physicochemical and biological consequences with applications*, edited by Y. Hatano, A. Mozumder (Marcel Dekker Inc, New York, 2004)
21. For a review see R.E. Palmer, in *Progress in Surface Science*, edited by S.G. Davison (Pergamon Press, New York, 1992)
22. For a review see L. Sanche, Mass. Spectrom. Rev. **21**, 349 (2002)
23. R.L.P. Adams, J.T. Knowler, D.P. Leader, *The biochemistry of the Nucleic Acids*, 10th edn. (Chapman and Hall, New York, 1981)
24. S. Swarts, M. Sevilla, D. Becker, C. Tokar, K. Wheeler, Radiat. Res. **129**, 333 (1992)
25. G. Leclerc, T. Goulet, P. Cloutier, J.-P. Jay-Gerin, L. Sanche, J. Phys. Chem. **91**, 4999 (1987)
26. I. Dabkowska, J. Rak, M. Gutowski, J.M. Nilles, S.T. Stokes, D. Radisic, K.H. Bowen, Phys. Chem. Chem. Phys. **6**, 4351 (2004)
27. H. Kang, C. Jouvet, C. Dedoner-Lardeux, S. Martrenchard, G. Gregoire, C. Desfrançois, J.P. Schermann, M. Barat, J.A. Fayeton, Phys. Chem. Chem. Phys. **7**, 394 (2005) and citations therein.
28. C. Desfrançois, H. Abdoul-Carime, J.P. Schermann, Int. J. Mod. Phys. B **10**, 1339 (1996)
29. F.A. Gianturco, R.R. Lucchese, J. Chem. Phys. **108**, 6144 (1998)
30. M.H.F. Bettega, C. Winstead, V. McKoy, J. Chem. Phys. **112**, 8806 (2000)
31. L.G. Caron, L. Sanche, Phys. Rev. Lett. **91**, 113201-1 (2003)
32. L.G. Caron, L. Sanche, Phys. Rev. A **70**, 032719-1 (2004)
33. D. Dill, J.L. Dehmer, J. Chem. Phys. **61**, 692 (1974)
34. J.B. Pendry, *Low Energy Electron Diffraction* (Academic, London, 1974)
35. R. Barrios, P. Skurski, J. Simons, J. Phys. Chem. B **106**, 7991 (2002)
36. J. Berdys, I. Anusiewicz, P. Skurki, J. Simons, J. Am. Chem. Soc. **126**, 6441 (2004)
37. J. Berdys, P. Skurski, J. Simons, J. Phys. Chem. B **108**, 5800 (2004)
38. J. Berdys, I. Anusiewicz, P. Skurki, J. Simons, J. Phys. Chem. A **108**, 2999 (2004)
39. X. Li, M.D. Sevilla, L. Sanche, J. Am. Chem. Soc. **125**, 13668 (2003)
40. X. Li, M.D. Sevilla, L. Sanche, J. Phys. Chem. B **108**, 5472 (2004)
41. X. Li, M.D. Sevilla, L. Sanche, J. Phys. Chem. B **108**, 19013 (2004)
42. X. Li, L. Sanche, M.D. Sevilla, J. Phys. Chem. A, **106**, 11248 (2002)
43. X. Li, M.D. Sevilla, L. Sanche, J. Am. Chem. Soc. **125**, 8916 (2003)
44. A. Grandi, F.A. Gianturco, N. Sanna, Phys. Rev. Lett. **93**, 048103-1 (2004)
45. F.A. Gianturco, R.R. Lucchese, J. Chem. Phys. **120**, 7446 (2004)
46. F.A. Gianturco, R.R. Lucchese, J. Phys. Chem. A **108**, 7056 (2004)
47. Ph. Bernhardt, W. Friedland, P. Jacob, H.G. Paretzke, Int. J. Mass Spectrom. **223-224**, 579 (2003)
48. P. Mozejko, L. Sanche, Radiat. Environ. Biophys. **42**, 201 (2003)
49. P. Mozejko, L. Sanche, Radiat. Phys. Chem. **73**, 77 (2005)
50. See for example, S. Denifl, S. Ptasińska, M. Probst, J. Hrušák, P. Scheier, T.D. Märk, J. Phys. Chem. A **108**, 6562 (2004)
51. K. Aflatooni, G.A. Gallup, P.D. Burrow, J. Phys. Chem. A **102**, 6205 (1998)

52. M.A. Hervé du Penhoat, M.A. Huels, P. Cloutier, J.P. Jay-Gerin, L. Sanche, J. Chem. Phys. **114**, 5755 (2001)
53. D.V. Klyachko, M.A. Huels, L. Sanche, Radiat. Res. **151**, 177 (1999)
54. B. Boudaïffa, P. Cloutier, D. Hunting, M.A. Huels, L. Sanche, Radiat. Res. **157**, 227 (2002)
55. L. Patthey, Ph.D. thesis, Université de Lausanne, 1995.
56. M. Nyberg, J. Hasselström, O. Karis, N. Wassdahl, M. Weinelt, A. Nilsson, L.G.M. Petterson, J. Chem. Phys. **112**, 5420 (2000)
57. M.D. Porter, T.B. Bright, D.L. Allara, C.E.D. Chidsey, J. Am. Chem. Soc. **109**, 3559 (1987)
58. S. Feil, K. Gluch, S. Matt-Leubner, P. Scheier, J. Limtrakul, M. Probst, H. Deutsch, K. Becker, A. Stamatovic, T.D. Märk, J. Phys. B: At. Mol. Opt. Phys. **37**, 3013 (2004)
59. K. Aflatooni, A.M. Scheer, P.D. Burrow, Chem. Phys. Lett. **408**, 426 (2005)
60. L. Sanche, M. Deschênes, Phys. Rev. Lett. **61**, 2096 (1988)
61. G.A. Kimmel, T.M. Orlando, Phys. Rev. Lett. **75**, 2606 (1995)
62. O. Rakhovskaia, P. Wiethoff, P. Feulner, Nucl. Instrum. Meth. B **101**, 169 (1995)
63. P. Dugal, M.A. Huels, L. Sanche, Radiat. Res. **151**, 325 (1999)
64. L. Sanche, Scanning Microsc. **9**, 619 (1995)
65. L. Sanche, M. Michaud, Phys. Rev. B **30**, 6078 (1984)
66. H. Ibach, D.L. Mills, *Electron Energy Loss Spectroscopy and Surface Vibration* (Academic, New York, 1982)
67. S.-P. Breton, M. Michaud, C. Jäggle, P. Swiderek, L. Sanche, J. Chem. Phys. **121**, 11240 (2004)
68. M. Lepage, M. Michaud, L. Sanche, J. Chem. Phys. **107**, 3478 (1997)
69. Z. Cai, P. Cloutier, D. Hunting, L. Sanche, J. Phys. Chem. B **109**, 4796 (2005)
70. S.G. Ray, S.S. Daube, R. Naaman, Proc. Natl. Acad. Sci. **102**, 15 (2005)
71. J. Sambrook, D.W. Russell, *Molecular Cloning: A laboratory manual* (Cold Spring Harbor, New York, 2001), Vol. 1, Chap. 5
72. J. Cadet et al., Free Radiat. Biol. Med. **33**, 441 (2002)
73. T. Solomun, E. Illenberger, Chem. Phys. Lett. **396**, 448 (2004)
74. M.A. Huels, B. Boudaïffa, D. Hunting, L. Sanche, A.J. Waker, in *Microdosimetry: An Interdisciplinary Approach*, edited by D.T. Goodhead, P. O'Neill, H.G. Menzel (Royal Society of Chemistry, Cambridge, UK, 1997)
75. B. Boudaiffa, P. Cloutier, D. Hunting, M.A. Huels, L. Sanche, Science **287**, 1658 (2000)
76. B. Boudaiffa, D.J. Hunting, P. Cloutier, M.A. Huels, L. Sanche, Int. J. Radiat. Biol. **76**, 1209 (2000)
77. Y. Zheng, P. Cloutier, J.R. Wagner, L. Sanche, Rev. Sci. Instrum. **75**, 4534 (2004)
78. S. Denifl, S. Ptasińska, G. Hanel, B. Gstir, M. Probst, P. Scheier, T.D. Märk, J. Chem. Phys. **120**, 6557 (2004)
79. G. Hanel, B. Gstir, S. Denifl, P. Scheier, M. Probst, B. Farizon, M. Farizon, E. Illenberger, T.D. Märk, Phys. Rev. Lett. **90**, 8104 (2003)
80. M.I. Sukhoviya, I.A. Petruschko, M.I. Shafranyosh, Book of Abstr. IX ECSBM, Prague, Czech Republic, 2001.

81. R. Abouaf, J. Pommier, H. Dunet, Int. J. Mass Spectrom. **226**, 397 (2003)
82. S. Denifl, S. Ptasińska, M. Cingel, S. Matejcik, P. Scheier, T.D. Märk, Chem. Phys. Lett. **377**, 74 (2003)
83. S. Gohlke, H. Abdoul-Carime, E. Illenberger, Chem. Phys. Lett. **380**, 595 (2003)
84. H. Abdoul-Carime, S. Gohlke, E. Illenberger, Phys. Rev. Lett. **92**, 168103-1 (2004)
85. S. Ptasińska, S. Denifl, V. Grill, T.D. Märk, P. Scheier, S. Gohlke, M.A. Huels, E. Illenberger, Angew. Chem. Int. Ed. **44**, 1657 (2005)
86. S. Denifl, B. Sonnweber, G. Hanel, P. Scheier, T.D. Märk, Int. J. Mass Spectrom. **238**, 47 (2004)
87. M.A. Huels, L. Parenteau, M. Michaud, L. Sanche, Phys. Rev. A **51**, 337 (1995)
88. H. Abdoul-Carime, P. Cloutier, L. Sanche, Radiat. Res. **155**, 625 (2001)
89. H. Abdoul-Carime, S. Gohlke, E. Fischbach, J. Scheike, E. Illenberger, Chem. Phys. Lett. **387**, 267 (2004)
90. Y. Zheng, P. Cloutier, D.J. Hunting, J.R. Wagner, L. Sanche, J. Am. Chem. Soc. **126**, 1002 (2004)
91. R. Abouaf, J. Pommier, H. Dunet, Chem. Phys. Lett. **381**, 486 (2003)
92. P.L. Lévesque, M. Michaud, L. Sanche, Nucl. Instrum. Meth. Phys. Res. B **208**, 225 (2003)
93. P.L. Lévesque, M. Michaud, W. Cho, L. Sanche, J. Chem. Phys. **122**, 224704 (2005)
94. P. Lévesque, M. Michaud, L. Sanche, J. Chem. Phys. **122**, 94701 (2005)
95. W. Cho, M. Michaud, L. Sanche, J. Chem. Phys. **121**, 11289 (2004)
96. S. Ptasińska, S. Denifl, P. Scheier, T.D. Märk, J. Chem. Phys. **120**, 8505 (2004)
97. D. Antic, L. Parenteau, M. Lepage, L. Sanche, J. Phys. Chem. **103**, 6611 (1999)
98. D. Antic, L. Parenteau, L. Sanche, J. Phys. Chem. B **104**, 4711 (2000)
99. M.A. Huels, L. Parenteau, L. Sanche, J. Phys. Chem. B **108**, 16303 (2004)
100. M. Lepage, S. Letarte, M. Michaud, F. Motte-Tollet, M.-J. Hubin-Franskin, D. Roy, L. Sanche, J. Chem. Phys. **109**, 5980 (1998)
101. X. Pan, L. Sanche, Phys. Rev. Lett. **94**, 198104 (2005)
102. M. Folkard, K.M. Prise, B. Vojnovic, S. Davies, M.J. Roper, B.D. Michael, Int. J. Radiat. Biol. **64**, 651 (1993)
103. B. Boudaïffa, P. Cloutier, D. Hunting, M.A. Huels, L. Sanche, Méd. Sci. **16**, 1281 (2000)
104. M.A. Huels, B. Boudaïffa, P. Cloutier, D. Hunting, L. Sanche, J. Am. Chem. Soc. **125**, 4467 (2003)
105. X. Pan, P. Cloutier, D. Hunting, L. Sanche, Phys. Rev. Lett. **90**, 208102-1 (2003)
106. X. Pan, H. Abdoul-Carime, P. Cloutier, A.D. Bass, L. Sanche, Radiat. Phys. Chem. **72**, 193 (2005)
107. F. Martin, P.D. Burrow, Z. Cai, P. Cloutier, D.J. Hunting, L. Sanche, Phys. Rev. Lett. **93**, 068101-1 (2004)
108. A. Scheer, K. Aflatooni, G.A. Gallup, P.D. Burrow, Phys. Rev. Lett. **92**, 8102 (2004)
109. D.M. Pearl, P.D. Burrow, J.J. Nash, H. Morrison, K.D. Jordan, J. Am. Chem. Soc. **115**, 9876 (1993)
110. D.M. Pearl, P.D. Burrow, J.J. Nash, H. Morrison, D. Nachtigallova, K.D. Jordan, J. Phys. Chem. **99**, 12379 (1995)

111. B.L. Henke, J.P. Knauer, K. Premaratne, J. Appl. Phys. **52**, 1509 (1981)
112. B.L. Henke, J.A. Smith, D.T. Attwood, J. Appl. Phys. **48**, 1852 (1977)
113. P.-C. Dugal, H. Abdoul-Carime, L. Sanche, J. Phys. Chem. B **104**, 5610 (2000)
114. H. Abdoul-Carime, P.-C. Dugal, L. Sanche, Radiat. Res. **153**, 23 (2000)
115. H. Abdoul-Carime, L. Sanche, Radiat. Res. **156**, 151 (2001)
116. H. Abdoul-Carime, L. Sanche, Int. J. Radiat. Biol. **78**, 89 (2002)
117. H. Abdoul Carime, P.C. Dugal, L. Sanche, Surf. Sci. **451**, 102 (2000)
118. T. Tanabe, K. Noda, M. Saito, E.B. Starikov, M. Tateno, Phys. Rev. Lett. **93**, 043201-1 (2004)
119. J. Ladik, H. Fruechtl, P. Otto, J. Jäger, J. Mol. Struct. **297**, 215 (1993)
120. C. Nogues, S.R. Cohen, S.S. Daube, R. Naaman, Phys. Chem. Chem. Phys. **6**, 4459 (2004)
121. R. Naaman, A. Haran, A. Nitzan, D. Evans, M. Galperin, J. Phys. Chem. B **102**, 3658 (1998)
122. S. Zamenhof, R. DeGiovanni, S. Greer, Nature **181**, 827 (1958)
123. J.D. Zimbrick, J.F. Ward, L.S. Myers Jr, Int. J. Radiat. Biol. **16**, 505 (1969)
124. L.D. Simpson, J.D. Zimbrick, Int. J. Radiat. Biol. **28**, 461 (1975)
125. L.L. Ling, J.F. Ward, Radiat. Res. **121**, 76 (1990)
126. M. Katouzian-Safadi, M. Charlier, J. Chim. Phys. **94**, 326 (1997)
127. H. Abdoul-Carime, M.A. Huels, F. Brüening, E. Illenberger, L. Sanche, J. Chem. Phys. **113**, 2517 (2000)
128. S. Denifl, S. Matejcik, B. Gstir, G. Hanel, M. Probst, P. Scheier, T.D. Märk, J. Chem. Phys. **118**, 4107 (2003)
129. H. Abdoul-Carime, M.A. Huels, E. Illenberger, L. Sanche, J. Am. Chem. Soc. **123**, 5354 (2001)
130. H. Abdoul-Carime, M.A. Huels, E. Illenberger, L. Sanche, Int. J. Mass Spectrom. **228**, 703 (2003)
131. M-A. Hervé du Penhoat, M.A. Huels, P. Cloutier, J.-P. Jay-Gerin, L. Sanche, Phys. Chem. Chem. Phys. **5**, 3270 (2003)
132. M-A. Hervé du Penhoat, M.A. Huels, P. Cloutier, J.-P. Jay-Gerin, L. Sanche, J. Phys. Chem. B **108**, 17251 (2004)
133. H. Abdoul-Carime, P. Limão-Vieira, S. Gohlke, I. Petrushko, N.J. Mason, E. Illenberger, Chem. Phys. Lett. **393**, 442 (2004)
134. S. Cecchini, S. Girouard, M.A. Huels, L. Sanche, D.J. Hunting, Radiat. Res. **162**, 604 (2004)
135. M. Sevilla, Radiat. Res. **162**, 603 (2004)
136. K. Aflatooni, B. Hitt, G.A. Gallup, P.D. Burrow, J. Chem. Phys. **115**, 6489 (2001)
137. H. Abdoul-Carime, S. Cecchini, L. Sanche, Radiat. Res. **158**, 23 (2002)
138. H. Abdoul-Carime, L. Sanche, J. Phys. Chem. B **106**, 12186 (2002)
139. S. Carles, F. Lecomte, J.P. Schermann, C. Desfrancois, S. Xu, J.M. Nilles, K.H. Bowen, J. Berges, C. Houée-Levin, J. Phys. Chem. A **105**, 5622 (2001)
140. H. Abdoul-Carime, L. Sanche, Radiat. Res. **160**, 86 (2003)
141. H. Abdoul-Carime, L. Sanche, J. Phys. Chem. B **108**, 457 (2004)
142. S. Ptasińska, S. Denifl, P. Candor, S. Matejcik, P. Scheier, T.D. Märk, Chem. Phys. Lett. **403**, 107 (2005)
143. H. Abdoul-Carime, S. Gohlke, E. Illenberger, Chem. Phys. Lett. **402**, 497 (2005)
144. S. Gohlke, A. Rosa, E. Illenberger, F. Brüning, M.A. Huels, J. Chem. Phys. **116**, 10164 (2002)
145. S. Ptasińska, S. Denifl, A. Abedi, P. Scheier, T.D. Märk, Anal. Bioanal. Chem. **377**, 1115 (2003)
146. H. Abdoul-Carime, E. Illenberger, Chem. Phys. Lett. **397**, 309 (2004)
147. H. Abdoul-Carime, S. Gohlke, E. Illenberger, Phys. Chem. Chem. Phys. **6**, 161 (2004)
148. H. Abdoul-Carime, E. Illenberger, Chem. Phys. Lett. **390**, 481 (2004)